INNATE IMMUNE SYSTEM

NKG2D-mediated detection of metabolically stressed hepatocytes by innate-like T cells is essential for initiation of NASH and fibrosis

Sonja Marinović[1]†, Maja Lenartić[1]†, Karlo Mladenić[1]†, Marko Šestan[1], Inga Kavazović[1], Ante Benić[1], Mia Krapić[1], Lukas Rindlisbacher[2], Maja Cokarić Brdovšak[3], Colin Sparano[2], Gioana Litscher[2], Tamara Turk Wensveen[4,5], Ivana Mikolašević[4], Dora Fŭkar Čupić[6], Lidija Bilić-Zulle[7], Aleksander Steinle[8], Ari Waisman[9], Adrian Hayday[10], Sonia Tugues[2], Burkhard Becher[2], Bojan Polić[1]*‡, Felix M. Wensveen[1]‡

Metabolic-associated fatty liver disease (MAFLD) is a spectrum of clinical manifestations ranging from benign steatosis to cirrhosis. A key event in the pathophysiology of MAFLD is the development of nonalcoholic steatohepatitis (NASH), which can potentially lead to fibrosis and hepatocellular carcinoma, but the triggers of MAFLD-associated inflammation are not well understood. We have observed that lipid accumulation in hepatocytes induces expression of ligands specific to the activating immune receptor NKG2D. Tissue-resident innate-like T cells, most notably γδ T cells, are activated through NKG2D and secrete IL-17A. IL-17A licenses hepatocytes to produce chemokines that recruit proinflammatory cells into the liver, which causes NASH and fibrosis. NKG2D-deficient mice did not develop fibrosis in dietary models of NASH and had a decreased incidence of hepatic tumors. The frequency of IL-17A$^+$ γδ T cells in the blood of patients with MAFLD correlated directly with liver pathology. Our findings identify a key molecular mechanism through which stressed hepatocytes trigger inflammation in the context of MAFLD.

INTRODUCTION

Metabolic-associated fatty liver disease (MAFLD), previously known as nonalcoholic fatty liver disease (NAFLD), is considered the hepatic manifestation of metabolic syndrome and affects about one-quarter of the global adult population (*1*–*3*). MAFLD is a spectrum of clinical entities ranging from simple steatosis to cirrhosis. Whereas many patients only suffer from benign steatosis [metabolic-associated fatty liver (MAFL)], some progress to nonalcoholic steatohepatitis (NASH). NASH is characterized by a marked increase in inflammatory cells in the liver, which drives the development of fibrosis and can ultimately cause cirrhosis and liver failure. Because of limited treatment options, MAFLD/NASH is quickly becoming one of the leading causes of liver-associated deaths worldwide. A better understanding of the molecular triggers that drive the transition of steatosis to hepatitis and cirrhosis is therefore imperative (*2*), but the early metabolic stress–specific signals that initiate inflammation in the liver remain largely unknown.

The pathophysiology of NASH is thought to require multiple triggers, including fat accumulation, gut microbiome disbalance, and oxidative stress (*2*), but the general consensus is that the key event in the transition of MAFL to NASH is the initiation of inflammation (*2*). The events leading up to inflammation are therefore of great clinical interest. CD4$^+$ T helper cell 17 (T_H17) cells and CD8$^+$ T cells have been shown to mediate NASH-associated liver fibrosis in both mice and humans (*4*–*8*). However, these cells are recruited in response to an established inflammatory milieu and therefore do not initiate immune cell accumulation in the liver. Instead, tissue-resident immune cells appear more likely to sense early metabolic stress and induce the inflammatory response (*9*). Innate-like T cells (ILTs), such as mucosa-associated invariant T (MAIT) cells and γδ T cells, have been shown to be involved in the pathophysiology of NASH. In humans and mice, NASH is associated with type 3 inflammation, characterized by the production of the cytokine interleukin-17A (IL-17A), most notably by MAIT cells and γδ T cells (*10*–*12*). In response to T cell receptor (TCR) engagement, these cells were shown to secrete IL-17A and promote liver fibrosis (*13*). However, TCR triggering alone is typically insufficient for the full activation of these cells (*14*), and engagement of other activating receptors through stress ligands usually plays a prominent role in immunosurveillance mediated by tissue-resident innate-like lymphocytes (*15*). The role of stress ligands in the development of NASH is currently unclear.

Several mechanisms have been associated with immune cell activation in response to metabolic stress. We have previously shown that hypertrophic adipocytes up-regulate ligands of the activating natural killer (NK) cell receptor NCR1 in obesity (*16*). As a response, tissue-resident NK cells proliferated and secreted interferon-γ (IFN-γ), which triggered macrophage polarization and local

[1]Department of Histology and Embryology, Faculty of Medicine, University of Rijeka, Rijeka, Croatia. [2]Institute of Experimental Immunology, University of Zürich, Zürich, Switzerland. [3]Center for Proteomics, Faculty of Medicine, University of Rijeka, Rijeka, Croatia. [4]Department of Internal Medicine, Faculty of Medicine, University of Rijeka, Rijeka, Croatia. [5]Center for Diabetes, Endocrinology and Cardiometabolism, Thallassotherapia, Opatija, Croatia. [6]Department of General Pathology and Pathological Anatomy, Faculty of Medicine, University of Rijeka, Rijeka, Croatia. [7]Clinical Department of Laboratory Diagnosis, Clinical Hospital Center Rijeka, Rijeka, Croatia. [8]Institute for Molecular Medicine, Goethe-University, Frankfurt am Main, Germany. [9]Institute for Molecular Medicine, University Medical Center of the Johannes Gutenberg University of Mainz, Mainz, Germany. [10]Department of Immunobiology, King's College London, London, UK.
*Corresponding author. Email: bojan.polic@uniri.hr
†These authors contributed equally to this work.
‡These authors contributed equally to this work.

inflammation (*16*). In the liver, hepatic stress caused by hepatitis B and C virus infection was associated with the induction of ligands for the activating receptor NKG2D (*17*, *18*). NKG2D is constitutively expressed on many immune cells, most notably innate and innate-like lymphocytes such as NK, MAIT, and γδ T cells, but its ligands are typically only induced in tissues in response to stress (*19*). Upon NKG2D engagement, immune cells mediate cytotoxic responses and/or produce cytokines, and this receptor has been shown to play a role in many pathologies (*19*, *20*). In a mouse model for hepatotoxicity mediated by injection of carbon tetrachloride, NKG2D ligands (NKG2D-Ls) were shown to be induced and could drive NK cell–mediated killing of hepatic stellate cells (*21*). However, whether NKG2D plays a functional role in NASH is currently unknown.

Here, we aimed to elucidate which molecular signal triggers MAFL-to-NASH transition in fatty liver disease. We observed that both induction of NKG2D-Ls and IL-17A expression correlate with the early stages of human NASH. Using a dietary model for NASH developed in our laboratory, we show that metabolic stress in hepatocytes promotes NKG2D-L expression, which is detected by tissue-resident ILTs, most notably γδ T cells. Their secretion of IL-17A early during disease pathogenesis in response to NKG2D engagement licenses hepatocytes to produce chemokines and attract proinflammatory myeloid cells. Deficiency of NKG2D or IL-17A receptor expression on hepatocytes resulted in a considerable reduction in liver inflammation and fibrosis. IL-17A expression by ILTs in the blood of patients with MAFLD correlated positively with liver pathology. Our findings identify a key molecular mechanism that mediates the transition of MAFL to NASH with potential applications as a diagnostic biomarker and therapeutic target.

RESULTS

MAFLD is associated with an increase of NKG2D-Ls and IL-17A–expressing cells in the human liver

Human MAFLD is associated with steatosis, inflammation, and fibrosis. We analyzed histological sections of liver biopsies from patients who were diagnosed with MAFLD to characterize disease progression. We observed that both steatosis and fibrosis often start in zone I of the liver lobules around the hepatic artery, where oxygenation is highest and most oxygen radicals are expected to be generated. From here, pathology spreads outward toward zone III (Fig. 1A). Late-stage steatosis and fibrosis were usually accompanied by diffuse foci of inflammatory cells, which are indicative of NASH.

MAFLD generates both metabolic and inflammatory stress in hepatocytes. We therefore investigated whether ligands of the activating stress receptor NKG2D are induced in liver tissue from patients with MAFLD. Immunohistochemical staining revealed that the NKG2D-Ls MICA/B are up-regulated specifically in sections most affected by steatosis compared with healthy sections of the same tissue (Fig. 1B and fig. S1A). We did not observe induction of the NKG2D-Ls ULBP1 or ULBP3 in livers of patients. MAFLD has been associated with type 3 inflammation, so we investigated whether IL-17A expression is induced in liver biopsy materials of patients with MAFLD and whether this correlates with the disease severity score (*22*). We observed that the frequency of IL-17A–expressing cells positively correlated with both the level of steatosis and liver inflammation (Fig. 1C). We observed that the increase in IL-17A–expressing cells highly correlated with the early stages of MAFLD (NAS scores of 3 to 5), whereas it decreased again in later stages of the disease (NAS scores of 6 and 7) (Fig. 1, C and D, and fig. S1B).

To determine which cells produce IL-17A in human livers, we first made use of publicly available single-cell RNA-sequencing data of human liver biopsy material (*23*). This showed that *Rorc*, the transcription factor mediating IL-17A expression, is predominantly expressed by T cells (fig. S1C). In addition, we found that *Rorc* was expressed in a subpopulation that also expressed *Klrk1*, the gene encoding NKG2D. To confirm that Rorc expression also translated into IL-17A production, immune cells were isolated from fresh biopsy material and stimulated in vitro with phorbol 12-myristate 13-acetate (PMA) and ionomycin. Cytokine-producing cells were identified by flow cytometry. We observed that IL-17A was almost exclusively produced by $CD3^+$ cells (Fig. 1E). Of these, most cells had a $CD4^+$ T_H17 profile. In addition, we observed that CD8 T cells and γδ T cells were prominent sources of IL-17A (Fig. 1F and fig. S1D).

In summary, we found that human MAFLD is associated with an up-regulation of NKG2D-Ls and an increase in the frequency of IL-17A–producing cells, especially in the early stages of the disease. This suggests that a causal relationship may exist between these two parameters.

Lipid accumulation in murine hepatocytes induces up-regulation of NKG2D-Ls

To gain mechanistic insight into early hepatic stress responses in the context of MAFLD, we established a mouse model for this disease. Current dietary models of MAFLD are typically based on the exclusion of key nutrients, such as choline and methionine, and are therefore not an ideal representation of human disease (*24*). We formulated a modified amylin liver NASH diet (*25*), which we termed the steatosis-steatohepatitis diet (SSD). SSD contains high levels of fat, fructose, and cholesterol and mimics an unhealthy Western lifestyle. SSD-fed mice rapidly gained body weight (Fig. 2A) and accumulated visceral adipose tissue (VAT) mass (fig. S2A), which is one of the hallmarks of metabolic syndrome. Compared with normal chow diet (NCD)–fed controls, SSD-fed animals displayed hepatomegaly and showed an increased liver–to–body weight ratio (Fig. 2B), a key feature of liver pathology in humans (*26*). We also observed an increase in the liver enzymes alanine transaminase (ALT) and aspartate transaminase (AST) in the serum, which are clinical markers of liver damage (Fig. 2C).

Histological analysis of murine liver samples from SSD-fed mice showed a gradual progression of fatty liver disease, which was highly similar to the pathology seen in humans. After 4 weeks of feeding, we observed glycogen-induced distension of hepatocytes, followed by moderate micro- and macrovesicular steatosis after 8 weeks (fig. S2B). As in human disease, pathology started in the periportal zone (zone I) and radiated outward. At 12 weeks of SSD feeding, livers showed widespread steatosis with inflammatory foci, cyst formation, and hepatocyte degeneration, indicating a transition from MAFL to NASH (fig. S2B). After 16 weeks, we could see advanced steatosis and considerable fibrosis in SSD-fed animals compared with NCD-fed controls, corresponding with NASH stage G3/F2 in humans (Figs. 1A and 2D). In addition, α–smooth muscle actin (αSMA) was strongly increased in SSD-fed mice, indicative of activated hepatic stellate cells (HSCs) and extracellular matrix

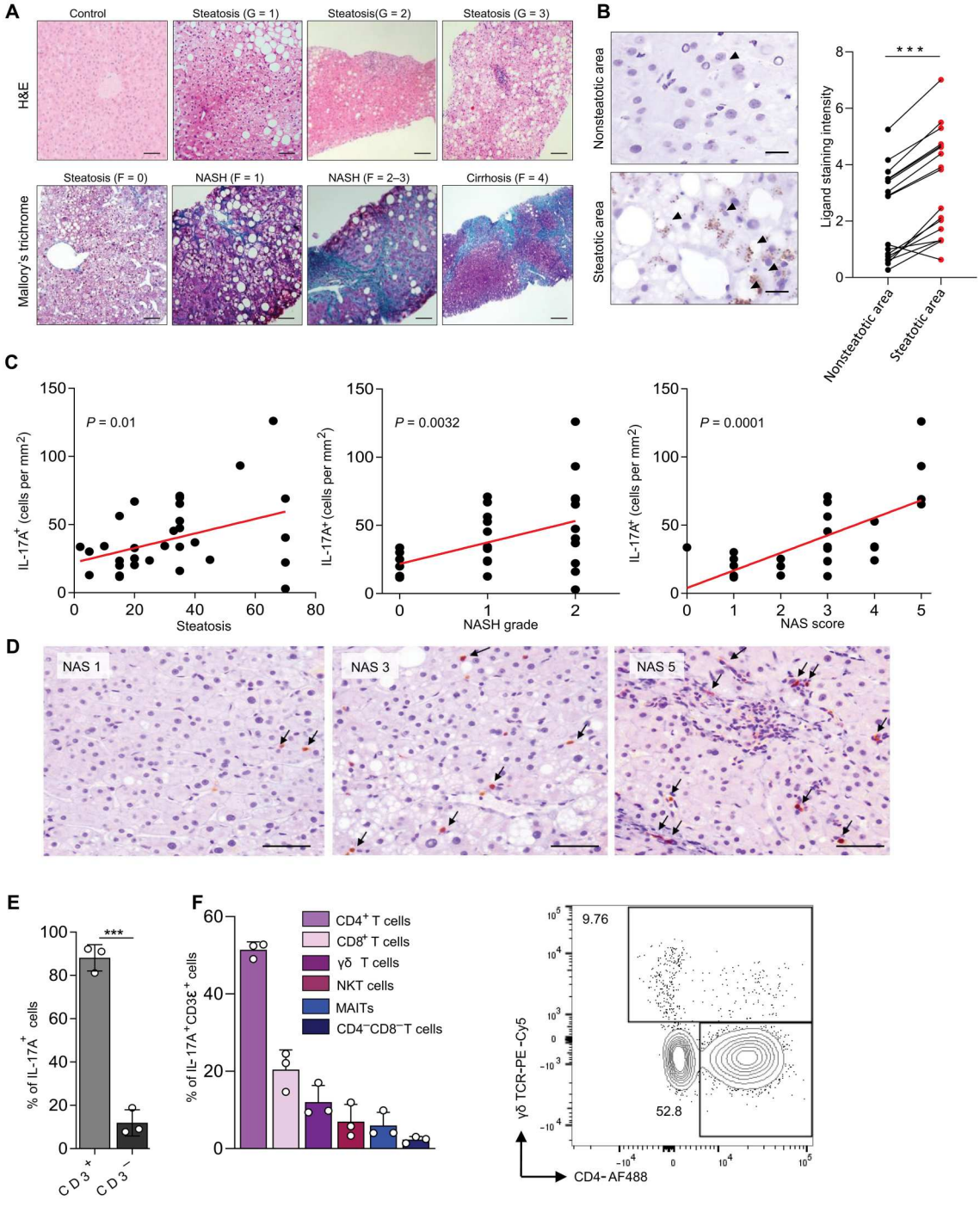

Fig. 1. MALFD is associated with an increase of NKG2D-Ls and IL-17A–expressing cells in the liver. (**A**) Representative histological slides of various stages of liver disease in human liver biopsies. (Top) Slides were stained with hematoxylin and eosin (H&E) and show a sample from a healthy individual and from patients with MAFLD with mild (G = 1), moderate (G = 2), or severe (G = 3) steatosis with ballooning and inflammation. (Bottom) Slides were stained with Mallory's trichrome and show liver tissue without fibrosis (F = 0) or with perisinusoidal and pericellular fibrosis without (F = 1) or together with extensive portal fibrosis (F = 2 to 3) or with cirrhosis (F = 4). Scale bars, 50 μm for control, steatosis (G = 1), steatosis (F = 0), and NASH (F = 1); 100 μm for steatosis (G = 2), steatosis (G = 3), and NASH (F = 2 to 3); and 250 μm for cirrhosis (F = 4). (**B**) Human biopsy material of patients with MAFLD was stained for the NKG2D-Ls MICA/B. Shown is NKG2D-L expression in steatotic and nonsteatotic regions within the same patient (n = 17). Scale bars, 20 μm. Arrowheads indicate a positive signal. (**C** and **D**) Human biopsy material of patients with MAFLD was stained for IL-17A. (C) The number of IL-17A–producing cells was correlated with the level of steatosis, grade of NASH, or the NAS-score (n = 35). (D) Representative staining for NAS scores 1, 3, and 5. Scale bars, 50 μm. (**E** and **F**) Quantification of IL-17A–producing cells in biopsies of human livers by flow cytometry. (**E**) Quantification of $CD3^+$ and $CD3^-$ cells within the $IL\text{-}17^+$ population (n = 3). (**F**) Quantification of IL-17A–producing T cells within the $CD3^+IL\text{-}17A^+$ cell pool (n = 3). Representative plot shows cells gated for $IL\text{-}17A^+CD3^+TCR\alpha V7.2^-CD56^-$. Statistical significance was determined by Wilcoxon signed-rank test (B), linear regression (C), or unpaired t test (E). Statistical significance was defined as $^*P < 0.05$, $^{**}P < 0.01$, and $^{***}P < 0.001$.

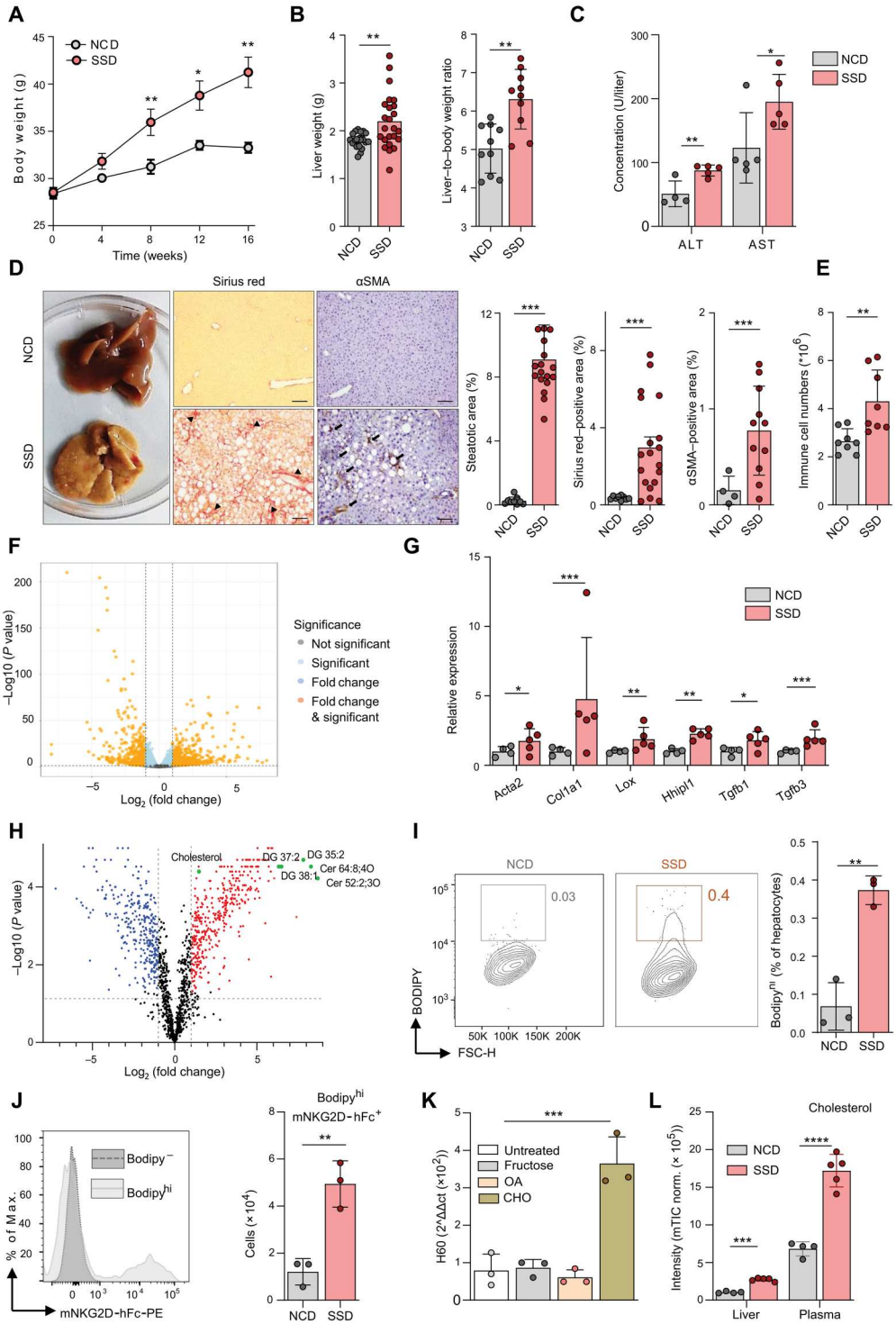

Fig. 2. Lipid accumulation in murine hepatocytes induces up-regulation of NKG2D-Ls. (A to E) WT mice were fed an SSD or an NCD for 2 to 16 weeks. (**A**) Total body weight over time ($n = 20$). (**B**) Liver weight and the liver–to–body weight ratio at 16 weeks ($n = 22$ to 24). (**C**) Serum AST and ALT levels after 16 weeks ($n = 5$). (**D**) Representative liver slides (200×) of fibrosis and HSC activation (αSMA) after 16 weeks of SSD feeding. Macroscopic changes in livers of SSD diet–fed mice showing yellow/gray firm parenchyma indicative for liver steatosis and fibrosis. Arrowheads indicate collagen accumulation. Arrows indicate αSMA$^+$ cells. Bar diagrams show the quantification of histology slides ($n = 4$ to 19). Scale bars, 20 μm. (**E**) Quantification of immune cells (CD45$^+$) in liver after 2 weeks determined by flow cytometry ($n = 8$). (F and G) Total liver lysates were analyzed by RNA sequencing after 3 weeks of NCD or SSD feeding ($n = 4$ or 5). (**F**) Volcano plot of differentially expressed genes. (**G**) Expression of key genes associated with liver fibrosis. (**H**) LC-MS/MS analysis of lipid species in the liver and plasma of mice fed for 18 days with NCD or SSD. (**I**) BODIPY staining of hepatocytes isolated from liver 2 weeks after initiation of SSD feeding ($n = 3$). (**J**) Quantification of NKG2D-L–expressing cells within BODIPY^{Bright} hepatocytes after 2 weeks of NCD or SSD feeding ($n = 3$). (**K**) Quantification of the NKG2D-L H60 by qPCR ($n = 3$) normalized to HPRT expression. (**L**) Levels of cholesterol in liver lysate and plasma samples of NCD- or SSD-fed mice determined by LC-MS/MS analysis. Shown are representative data of at least two experiments or pooled data of two independent experiments (A, B, and D). Shown are means ± SEM. Statistical significance was determined by unpaired *t* test (A to J and L) and ANOVA with Bonferoni posttesting (K). Statistical significance was defined as $^*P < 0.05$, $^{**}P < 0.01$, and $^{***}P < 0.001$.

deposition (Fig. 2D). Last, in accordance with our histological findings, SSD feeding caused a progressive increase of immune cells in the liver. Unexpectedly, this increase was already apparent 2 weeks after the initiation of feeding, suggesting that changes in the immunological microenvironment occur very early during development of NASH (Fig. 2E and fig. S2C).

To elucidate the molecular changes underlying SSD-induced liver pathology early in the disease before apparent inflammation, RNA-sequencing analysis was performed on total liver lysates of mice fed for 3 weeks with SSD. A total of 1386 transcripts were more than twofold differentially expressed between the groups, of which 969 were up-regulated and 417 were down-regulated in SSD-fed animals compared with NCD-fed controls (Fig. 2F).

Among the pathways that were most affected by SSD feeding, several were associated with metabolism and inflammation, further confirming the validity of SSD feeding as a model for NASH (fig. S2, D and E). Last, the analysis of individual transcripts showed that many putative genes associated with liver fibrosis, such as *Acta2*, *Col1a1*, *Lox*, and *Hhipl1*, were up-regulated in animals fed with SSD (Fig. 2G). Hepatic fibrosis was still observed in SSD-fed animals in which abdominal fat was surgically removed (fig. S2F), indicating that the liver is the primary source of stress signals inducing NASH.

We considered that liver inflammation after SSD feeding is induced by hepatocyte death caused by accumulation of toxic lipid species. Therefore, we analyzed the lipid profile of livers of animals fed for 3 weeks with an SSD or NCD by mass spectrometry. We observed an increase of several lipid species previously associated with lipotoxicity, including ceramides and diacylglycerols (Fig. 2H and table S1). However, levels of extracellular HMGB1, a marker associated with necrotic cell death, were not increased early after initiation of SSD feeding (fig. S2G). In addition, granulomas, which mark sites of necrotic cell death, were not observed after 4 weeks of SSD feeding (fig. S2H). Only after at least 8 to 16 weeks of SSD feeding could we detect signs of inflammatory cell death (fig. S2, G and H). Thus, lipotoxicity does not appear to be a major cause of liver inflammation at early stages of MAFLD in the SSD model.

We next hypothesized that metabolic stress initiates liver inflammation through the activation of NKG2D. We measured NKG2D-Ls on metabolically stressed hepatocytes. The lipid content of hepatocytes was visualized using BODIPY staining, and steatotic cells could be identified as BODIPY^{High} by flow cytometry (Fig. 2I). After 2 weeks of SSD feeding, steatotic cells showed significantly more expression of NKG2D-Ls ($P = 0.0047$) than hepatocytes isolated from NCD-fed controls by NKG2D-Fc staining (Fig. 2J). To determine which factor from the SSD diet drives NKG2D-L expression, we generated cultures of primary mouse hepatocytes and loaded them for 48 hours with fructose, cholesterol, or oleic acid. Whereas oleic acid was most notably associated with lipid accumulation in hepatocytes, cholesterol was most effective at inducing NKG2D-L expression, in particular of H60 (Fig. 2K and fig. S2, I and J).

Levels of cholesterol were highly increased in both the livers and the plasma of SSD-fed mice (Fig. 2L). To demonstrate its importance for the development of hepatitis in vivo, we subjected mice to an SSD diet in which cholesterol was omitted. This diet did not lead to inflammation in vivo (fig. S2K). In addition, feeding of mice with a diet containing high levels of fat [high-fat diet (HFD)], an established model for obesity-induced VAT inflammation and insulin resistance, resulted in obesity, hyperinsulinemia, and glucose intolerance (*27*), but we detected only mild steatosis and no signs of liver fibrosis (fig. S2, L and M). Conversely, animals fed with a diet rich in cholesterol [high-cholesterol diet (HCD)] did show immune cell accumulation in the liver (fig. S2N). However, HCD feeding did not cause steatosis or fibrosis (fig. S2, L and M), confirming previous observations (*28*) that the pathophysiology of NASH requires the cumulative impact of several metabolites. In summary, SSD feeding is a valid model for human NASH and causes NKG2D-L induction in hepatocytes after cholesterol accumulation.

NKG2D engagement is essential for the development of liver fibrosis in the context of NASH

To determine whether NKG2D signaling is essential for the induction of fibrosis in our model for NASH, we fed NKG2D-deficient (*Klrk1*$^{-/-}$) mice (*29*) with an SSD diet and analyzed the level of collagen deposition after 16 weeks. We found a notable reduction in the level of fibrosis in livers of *Klrk1*$^{-/-}$ mice compared with wild-type (WT) C57BL/6J controls, whereas steatosis was not greatly affected (Fig. 3A). Immunohistological staining of αSMA also showed a strong reduction of its expression in *Klrk1*$^{-/-}$mice (Fig. 3B). In most immune cells, NKG2D uses the DAP10 adaptor molecule to mediate intracellular signaling (*19*). To confirm the importance of NKG2D signaling in NASH progression, we placed DAP10-deficient (*Hcst*$^{-/-}$) mice on an SSD. After 16 weeks, we compared the liver pathology in DAP10-deficient mice with that of SSD-co-fed WT animals. The level of fibrosis and the αSMA expression in livers of *Hcst*$^{-/-}$ mice were both substantially reduced in comparison with WT mice. In contrast, levels of steatosis were not different between the SSD-fed groups of mice (Fig. 3C and fig. S3A).

NASH strongly increases the overall risk of developing cirrhosis and hepatocellular carcinoma (HCC) (*2*). Previously, NKG2D-mediated inflammation was shown to promote development of HCC (*30*). We therefore investigated the impact of NKG2D deficiency on long-term SSD feeding. WT (gray bar) and *Klrk1*$^{-/-}$ (blue bar) mice were placed on SSD for 1 year before analysis of hepatic pathology. Liver damage was significantly reduced in *Klrk1*$^{-/-}$ mice, as shown by much lower levels of ALT in circulation ($P = 0.0113$) (Fig. 3D). Histochemical analysis revealed that virtually all parameters associated with NASH, including NASH score, fibrosis, αSMA induction, and leukocyte infiltrations, were reduced in *Klrk1*$^{-/-}$ mice compared with WT controls (Fig. 3, E and F). Proliferation of cells, as determined by Ki67 staining, was predominantly observed within CD45^{+} immune cells and was significantly reduced in the livers of NKG2D-deficient animals ($P = 0.0245$) (Fig. 3, G and H), which is in line with reduced immune cell activation in this tissue. Last, the incidence of tumors, which was about 25% in livers of 1-year SSD-fed WT animals, was more than twofold reduced in the livers of *Klrk1*$^{-/-}$ mice, as was the average tumor size at the time point of analysis (Fig. 3I and fig. S3, B and C). Together, we conclude that NKG2D plays an important role in the development of NASH and long-term liver disease in the context of MAFLD.

Liver fibrosis in the context of NASH is mediated by ILTs

NKG2D is expressed on various lymphocyte subsets. We therefore determined which immune cells in the liver express NKG2D and whether expression changes in response to SSD feeding. CD11b^{+} myeloid cells did not express NKG2D, and expression was also very low on adaptive immune cells. In contrast, MAIT, CD3^{+}CD4^{-}CD8^{-} double-negative (DN) T cells, NKT, γδ T cells, and NK cells expressed high levels of NKG2D, and for the latter four, its expression was further increased in response to a NASH-inducing diet (Fig. 4A and fig. S4A). Further analysis revealed that all NKG2D-expressing cells also increased in absolute numbers upon 2 weeks of SSD feeding, relative to NCD-fed controls (fig. S4B).

To identify which of these cell populations contributes to the development of NKG2D-mediated NASH, we made use of several genetically modified mouse lines. First, we generated NK cell–specific NKG2D-deficient mice by crossing *Ncr1*^{Cre} mice with *Klrk1*$^{fl/fl}$

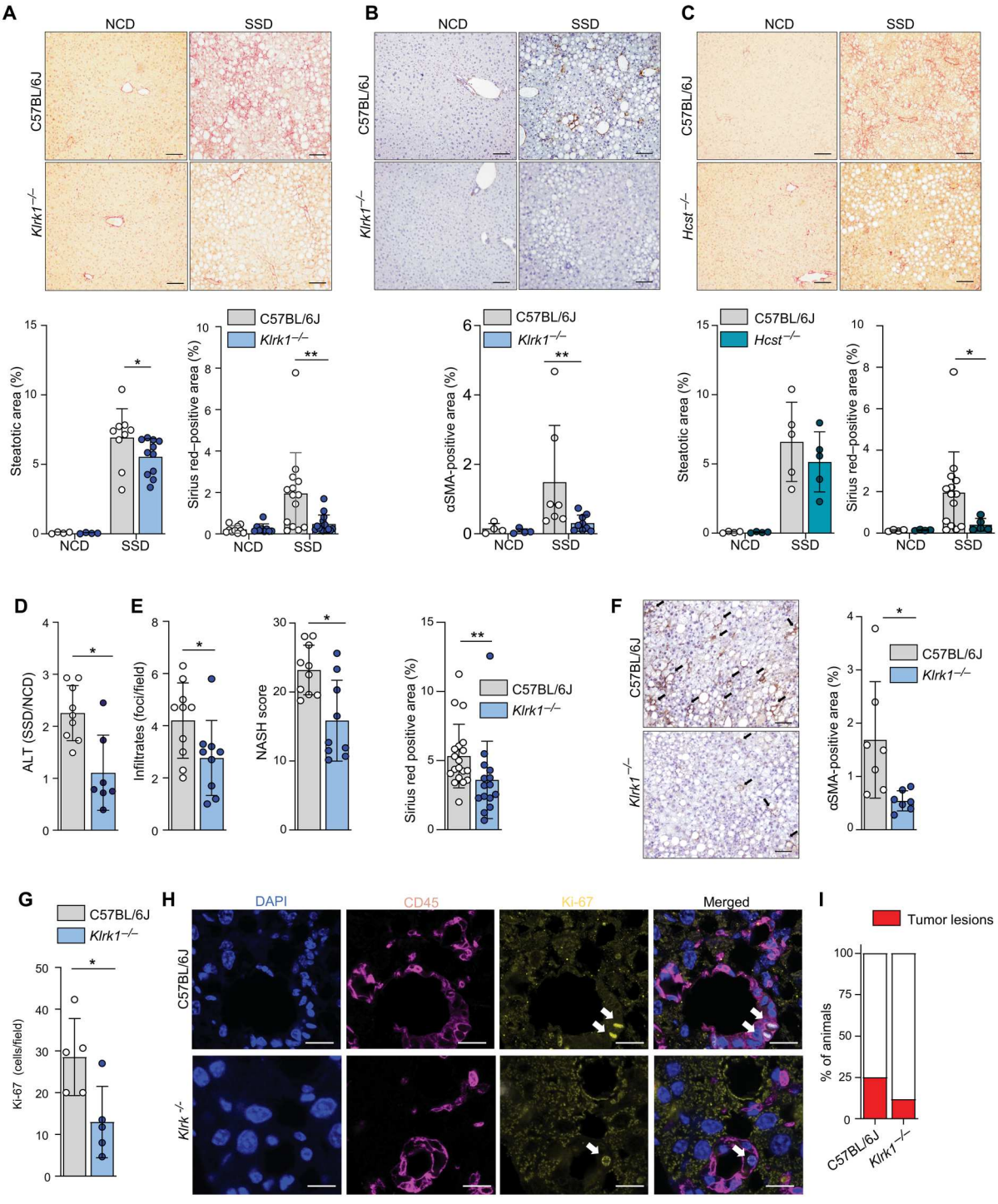

Fig. 3. NKG2D engagement is essential for development of liver fibrosis in context of NASH. (A and B) WT and *Klrk1*$^{-/-}$ (NKG2D-deficient) mice were fed an NCD or an SSD diet for 16 weeks ($n = 4$ to 11). (**A**) (Top) Representative liver slides stained with Sirius red (200×) and (bottom) quantification of steatosis and fibrosis. Scale bars, 100 μm. (**B**) (Top) Representative liver slides stained for αSMA and (bottom) quantification of HSC activation (200×). Scale bars, 100 μm. (**C**) WT and *Hcst*$^{-/-}$ (DAP10-deficient) mice were fed an NCD or an SSD diet for 16 weeks. (Top) Representative liver slides stained with Sirius red (200×) and (bottom) quantification of steatosis and fibrosis by Sirius red staining. Scale bars, 100 μm ($n = 4$ or 5). (D to I) WT and *Klrk1*$^{-/-}$ mice were fed an NCD or an SSD diet for 52 weeks, and livers were analyzed ($n = 7$ to 9). (**D**) Quantification of ALT in serum. (**E**) Quantification of liver pathology of histological slides stained with H&E or Sirius red. (**F**) (Left) Representative liver slides stained for αSMA and (right) quantification of HSC activation (200×). Scale bars, 100 μm. (**G**) Slides were stained for Ki67, and positive cells per field of view were quantified. (**H**) Representative immunofluorescence staining of CD45 and Ki67. Arrows mark Ki67^{+} nuclei. Scale bars, 10 μm. (**I**) The numbers of mice carrying macroscopically visible tumors were quantified ($n = 17$ to 20). The data are representative of at least two independent experiments or show pooled data of two experiments. Shown are means ± SEM. Statistical significance was determined by unpaired *t* test. Statistical significance was defined as $^{*}P < 0.05$, $^{**}P < 0.01$, and $^{***}P < 0.001$.

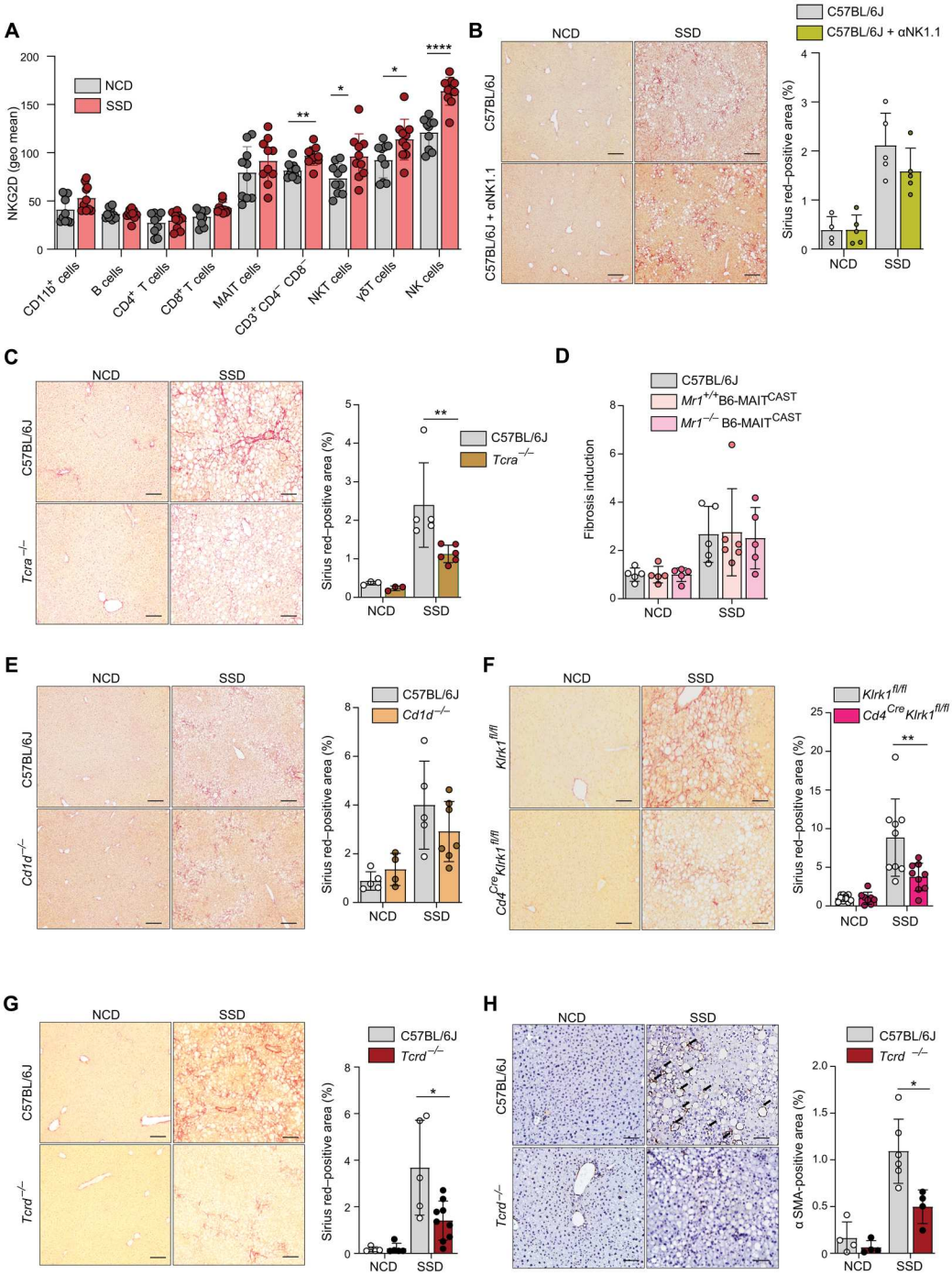

Fig. 4. Liver fibrosis in the context of NASH is mediated by ILTs. (**A**) WT mice were fed with an NCD or SSD for 18 days, and NKG2D expression was quantified in key hepatic leukocyte populations by flow cytometry ($n = 5$). (**B**) WT mice and C57BL/6J mice treated with NK cell–depleting antibody on a weekly basis were fed an NCD or an SSD diet for 16 weeks. Shown are (left) representative liver slides stained with Sirius red (200×) and (right) quantification of fibrosis ($n = 4$ or 5). (**C**) WT and *Tcra*$^{-/-}$ (TCR α-chain–deficient) mice were fed an NCD or an SSD diet for 16 weeks. Shown are (left) representative liver slides stained with Sirius red (200×) and (right) quantification of fibrosis ($n = 5$). (**D**) WT, *Mr1*$^{+/+}$B6-MAIT^{CAST}, and *Mr1*$^{-/-}$B6-MAIT^{CAST} mice were fed an NCD or an SSD diet for 16 weeks. Quantification of fibrosis is shown ($n = 5$ or 6). (**E**) WT and *Cd1d*$^{-/-}$ mice were fed an NCD or an SSD diet for 16 weeks. Shown are (left) representative liver slides stained with Sirius red (200×) and (right) quantification of fibrosis ($n = 4$ to 7). (**F**) *CD4*^{Cre}*Klrk1*$^{Flox/Flox}$ and *Klrk1*$^{Flox/Flox}$ littermate controls were fed an NCD or an SSD diet for 16 weeks. Shown are (left) representative liver slides stained with Sirius red (200×) and (right) quantification of fibrosis ($n = 9$ or 10). (G and H) WT and *Tcrd*$^{-/-}$ (TCR δ-chain–deficient) mice were fed an NCD or an SSD diet for 16 weeks ($n = 4$ to 10). (**G**) Shown are (left) representative liver slides stained with Sirius red (200×) and (right) quantification of fibrosis. (**H**) Shown are (left) representative liver slides stained for αSMA and (right) quantification of HSC activation (200×). Scale bars, 100 μm. The data are representative of at least two independent experiments or pooled data of at least two experiments (A and F). Shown are means ± SEM. Statistical significance was determined by unpaired *t* test. Statistical significance was defined as $^{*}P < 0.05$, $^{**}P < 0.01$, and $^{***}P < 0.001$.

animals (*31*) and placed them on an SSD for 16 weeks. Histological analysis of liver slides showed that *Ncr1*^{cre}*Klrk1*$^{fl/fl}$ and *Klrk1*$^{fl/fl}$ littermates had similar levels of liver fibrosis (fig. S4C). Furthermore, NK cell depletion did not impair fibrosis development in SSD-fed mice, excluding a role for these cells in the development of NASH in this model (Fig. 4B).

Apart from NK cells, NKG2D was highly expressed on the TCRα^{+} subsets MAIT cells, NKT cells, and CD4^{-}CD8^{-} DN T cells in the liver. We therefore investigated the importance of these cells in the development of liver fibrosis. Mice with genetic deficiency for the α-chain of the TCR were placed on SSD, and collagen deposits were quantified after 16 weeks. We observed that fibrosis was significantly reduced in these animals ($P = 0.0043$), although not to the levels of NCD-fed animals (Fig. 4C). Steatosis was not affected in these mice, suggesting an impact on inflammation but not on hepatic metabolism (fig. S4D). To determine which NKG2D^{+}TCRα^{+} T cell subset mediates SSD-induced liver fibrosis, we first investigated the role of MAIT cells. We made use of

MAIT^{CAST} mice, which contain about 10-fold more MAIT cells than WT controls. MAIT cells recognize antigen presented in the context of the nonclassical major histocompatibility complex molecule MR1. Animals deficient for this molecule therefore do not have MAIT cells (*32*). WT, *Mr1*$^{+/+}$ B6-MAIT^{CAST}, and *Mr1*$^{-/-}$ B6-MAIT^{CAST} animals were placed on an SSD, and liver fibrosis was determined after 16 weeks. Neither the absence nor the increased presence of MAIT cells resulted in a change in the level of liver fibrosis (Fig. 4D). We therefore conclude that MAIT cells do not contribute to the development of fibrosis in the SSD model.

The vast majority of NKT cells in liver are CD1d restricted (*33*). To investigate the role of NKT cells in NASH, *Cd1d*$^{-/-}$ mice were placed on an SSD for 16 weeks and liver fibrosis was analyzed. We did not observe a significant reduction in the amount of fibrosis in these animals compared with WT controls (Fig. 4E). Thus, CD1d-restricted NKT cells do not play a role in the development of SSD-induced NASH. Last, we wanted to investigate the role of DN T cells in the development of SSD-induced NASH. Unfortunately, the lack of cell-specific markers does not allow targeting of only this immune cell subset. However, all TCRα^{+} cells go through a CD4^{+} phase during thymic development. Because we excluded a role for MAIT and CD1d-restricted NKT cells in development of SSD-induced NASH, we therefore made use of Cd4^{cre}*Klrk1*$^{fl/fl}$mice. Cd4^{cre}*Klrk1*$^{fl/fl}$ mice and *Klrk1*$^{fl/fl}$ littermates were placed on an SSD, and liver fibrosis was quantified after 16 weeks. We observed a significant reduction of fibrosis in the livers of *Cd4*^{cre}*Klrk1*$^{fl/fl}$ animals compared with *Klrk1*$^{fl/fl}$ littermates (P = 0.0048), which was comparable to that observed in TCRα$^{-/-}$ mice (Fig. 4, C and F). Steatosis was not affected in these animals (fig. S4E). Thus, our findings indicate that DN T cells are important for NKG2D-dependent liver fibrosis in the context of NASH.

Neither CD4^{cre}*Klrk1*$^{fl/fl}$ nor TCRα$^{-/-}$ mice showed a complete abrogation of liver fibrosis after SSD feeding. We therefore hypothesized that γδ T cells also contribute to NKG2D-mediated liver fibrosis in our NASH model. Unfortunately, no model is available to specifically target genes in γδ T cells because the existent *Tcrd*^{CreERt2} model has very poor efficiency in the liver (*34*). Therefore, to determine the importance of γδ T cells in SSD-induced liver pathology, we made use of TCRδ$^{-/-}$ mice, which lack all γδ T cells. After 16 weeks of SSD feeding, TCRδ$^{-/-}$ animals showed a significant reduction in liver fibrosis compared with WT controls (P = 0.029), whereas steatosis was not affected (Fig. 4G and fig. S4F). In addition, αSMA expression was significantly lower in the livers of SSD-fed TCRδ$^{-/-}$ mice (P = 0.0137) (Fig. 4H). In summary, NKG2D-mediated liver fibrosis in the context of MAFLD is mediated by the concerted action of DN αβ T cells and γδ T cells.

NKG2D mediates liver fibrosis through IL-17A induction

NKG2D can mediate both cytotoxicity and cytokine production of NK cells and ILTs (*19*, *35*). We therefore investigated which signaling pathways are most affected by NKG2D deficiency early after initiation of metabolic stress induced by SSD feeding. RNA sequencing of total liver lysates revealed 496 transcripts that were differentially expressed at least twofold between WT and *Klrk1*$^{-/-}$ mice after 3 weeks of SSD feeding. Of these, 39 showed higher and 457 showed lower expression in NKG2D-deficient animals (Fig. 5A). When we performed a Kyoto Encyclopedia of Genes and Genomes (KEGG) pathway analysis on differentially expressed genes, we observed that the IL-17A receptor and the chemokine signaling pathways were among the most negatively affected in *Klrk1*$^{-/-}$ animals (Fig. 5B). Analysis of individual genes reveled that several transcriptional targets of the IL-17A receptor signaling pathway, including chemokines such as *Cxcl1*, *Cxcl2*, and *Ccl2*, were strongly reduced in SSD-fed NKG2D-deficient animals compared with WT controls (Fig. 5C). Inflammatory pathways were not affected in NCD-fed *Klrk1*$^{-/-}$ mice compared with WT controls (fig. S5, A and B). We therefore hypothesized that NKG2D-dependent induction of IL-17A expression mediates liver fibrosis in the context of MAFLD. To confirm this, we first determined the importance of IL-17A in the pathology of SSD-induced NASH. Analysis of cytokine expression by hepatic lymphocytes showed that IL-17A levels were rapidly and strongly increased after initiation of SSD feeding and stayed high for the duration of the experiment. In contrast, expression of IFN-γ and tumor necrosis factor (TNF) was not affected by SSD-induced metabolic stress (Fig. 5D and fig. S5C). IL-17A levels did not increase after HFD feeding, indicating that this cytokine may be specifically involved in the induction of liver fibrosis (fig. S5D).

IL-17A is important for several homeostatic processes, including maintenance of gut barrier integrity and adipose tissue metabolism (*36*, *37*). We therefore made use of *Il17ra*$^{fl/fl}$ mice to abrogate IL-17A sensitivity of specific cells. First, we crossed *Il17ra*$^{fl/fl}$ mice with lysozyme^{Cre} (*Lys*^{Cre}) animals to eliminate the IL-17A receptor in macrophages (*Il17ra*^{ΔMϕ}). However, *Il17ra*^{ΔMϕ} mice showed a similar level of fibrosis after 16 weeks of SSD feeding as *Il17ra*$^{fl/fl}$ littermate controls, indicating that IL-17A does not directly target these cells (Fig. 5E). IL-17A was shown to directly activate HSCs in a mouse model of NASH (*13*). We therefore crossed *Il17ra*$^{fl/fl}$ mice with GFAP^{Cre} animals, which eliminates the IL-17A receptor from HSCs and cholangiocytes (*38*). Sixteen weeks of SSD feeding did not show differences in liver fibrosis between *Il17ra*^{ΔHSC} mice and littermate controls (Fig. 5F). Last, we questioned whether IL-17A might directly target hepatocytes. To demonstrate this, *Il17ra*$^{fl/fl}$ mice were crossed with albumin^{Cre} (*Alb*^{Cre}) animals to generate *Il17ra*^{ΔHep} mice. After 16 weeks of SSD feeding, we observed a significant reduction in the amount of fibrosis in livers of animals with hepatocyte-specific deficiency for the IL-17A receptor compared with littermate controls (P = 0.0012) (Fig. 5G). The level of steatosis was comparable between groups, indicating an impact on inflammation rather than on hepatic metabolism (fig. S5E). In summary, metabolic stress of the liver leads to increased expression of IL-17A by leukocytes in this organ, which directly targets hepatocytes.

NKG2D stimulation promotes IL-17A production by hepatic γδ T cells in the context of NASH

Our findings indicate that in the context of MAFLD, γδ T cells and a subset of TCRα^{+} cells are responsible for the induction of liver fibrosis in response to NKG2D stimulation. We therefore investigated which of these cells produce IL-17A early after initiation of SSD feeding. In vitro restimulation of hepatic leukocytes isolated from the liver 2 weeks after initiation of SSD feeding showed that IL-17A is produced almost exclusively by T cells (Fig. 6A). Further analysis of immune cell subsets within the IL-17A^{+} population indicated that this cytokine is predominantly secreted by CD4^{+} T$_{H}$17, CD3^{+}CD4^{-}CD8^{-} T cells, and γδ T cells. Of these, only IL-17A–producing γδ T cells increased significantly upon SSD feeding (P = 0.0079) (Fig. 6B and fig. S6A). NKT cells were not a major source

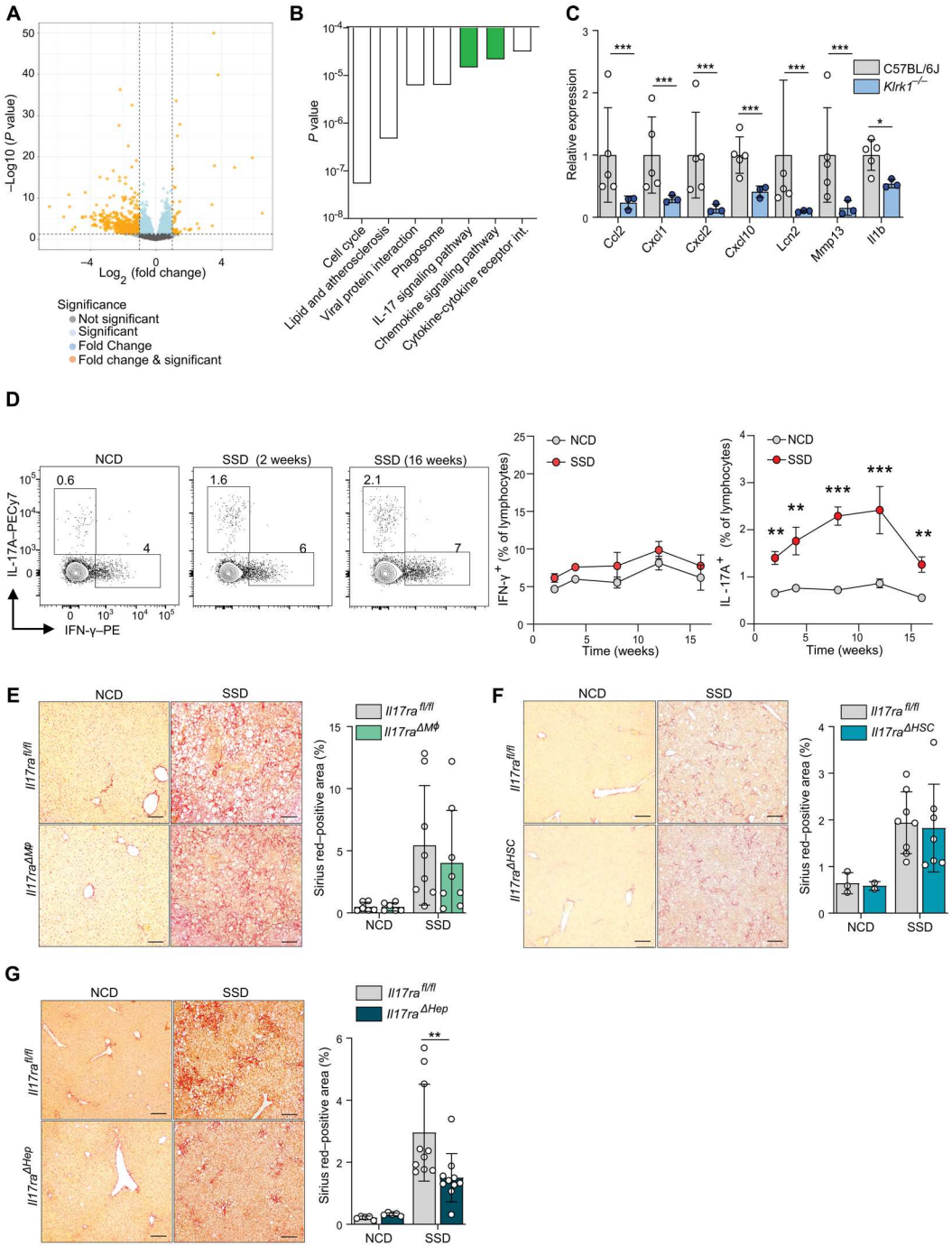

Fig. 5. IL-17A signaling to hepatocytes drives liver fibrosis in the context of NASH. (A to C) WT and *Klrk1* $^{-/-}$ mice were fed an SSD for 3 weeks, and the total transcriptome of liver tissue was analyzed by RNA sequencing. (**A**) Volcano plot of genes differentially expressed between WT and *Klrk1* $^{-/-}$ mice (n = 3 to 5). (**B**) Most down-regulated KEGG pathways in *Klrk1*$^{-/-}$ mice compared with WT controls by *P* value. Marked in green are the IL-17A receptor signaling pathway and the chemokine signaling pathway. (**C**) Differential expression of downstream target genes of the IL-17A receptor signaling pathway. (**D**) WT mice were fed with an NCD or SSD diet. At indicated time points, liver leukocytes were restimulated in vitro with PMA/ionomycin and cytokine production was measured by flow cytometry (n = 10). Representative plots are gated for lymphocytes. Numbers represent the percentage of IFN-γ or IL-17A–producing cells. (Right) Kinetics of hepatic IFN-γ– and IL-17A–producing lymphocytes over time. (**E**) *Il17ra*$^{fl/fl}$ and Lys^{Cre}*Il17ra*$^{fl/fl}$ (*Il17ra*$^{\Delta M\phi}$) littermates were fed an NCD or an SSD diet for 16 weeks. Shown are (left) representative liver slides stained with Sirius red (200×) and (right) quantification of fibrosis (n = 8). (**F**) *Il17ra*$^{fl/fl}$ and GFAP^{Cre}*Il17ra*$^{fl/fl}$ (*Il17ra*$^{\Delta HSC}$) littermates were fed an NCD or an SSD diet for 16 weeks. Shown are (left) representative liver slides stained with Sirius red (200×) and (right) quantification of fibrosis (n = 2 to 7). (**G**) *Il17ra*$^{fl/fl}$ and albumin^{Cre}*Il17ra*$^{fl/fl}$ (*Il17ra*$^{\Delta Hep}$) littermates were fed an NCD or an SSD diet for 16 weeks. Shown are (left) representative liver slides stained with Sirius red (200×) and (right) quantification of fibrosis (n = 5). Scale bars, 100 μm (E to G). The data are representative of at least two independent experiments or pooled data of at least two experiments (D to G). Shown are means ± SEM. Statistical significance was determined by unpaired t test. Statistical significance was defined as *P < 0.05, **P < 0.01, and ***P < 0.001.

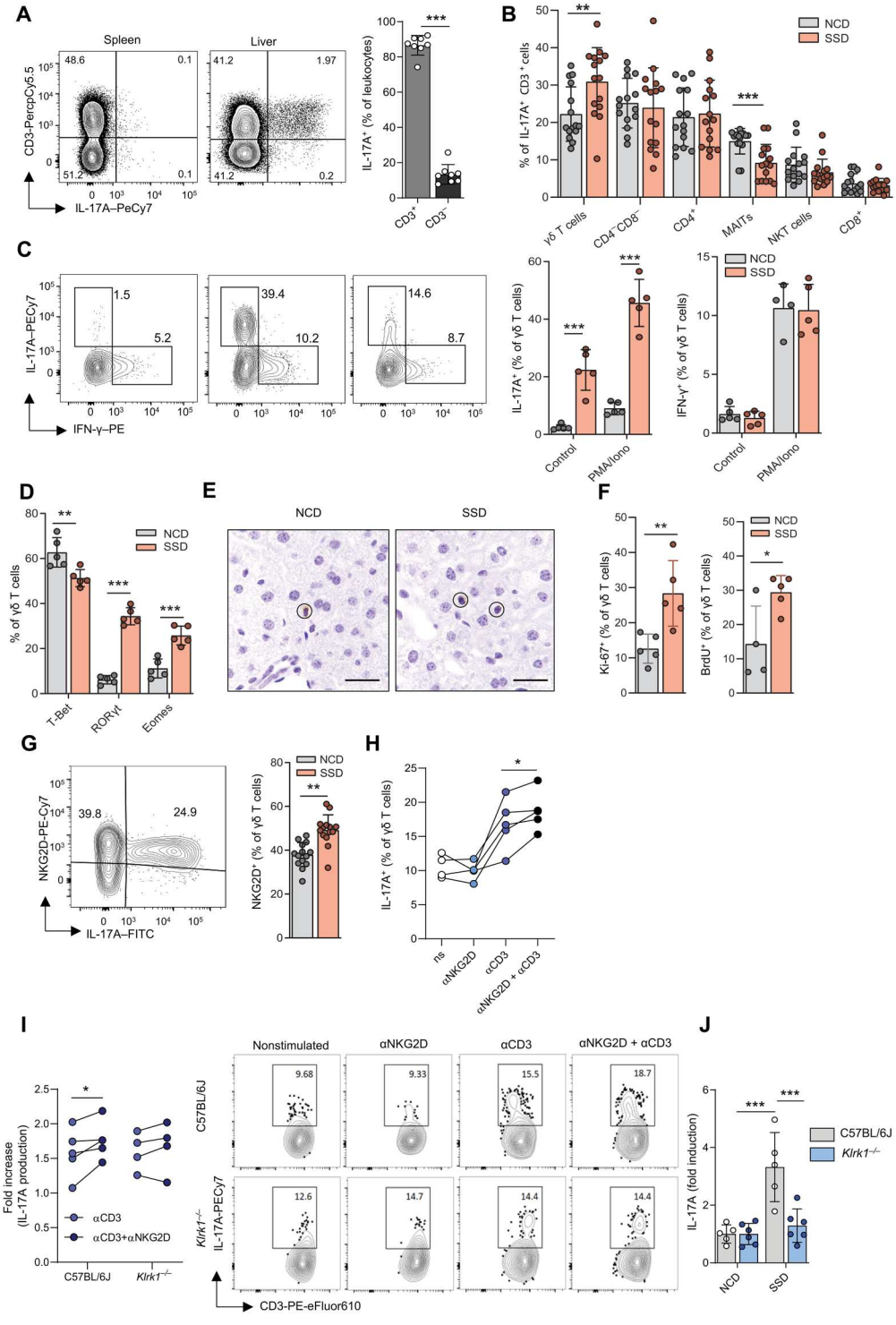

Fig. 6. Liver fibrosis in context of NASH is mediated by ILTs. (A and B) WT mice were fed with an NCD or SSD diet and after 18 days liver leukocytes were restimulated in vitro with PMA/ionomycin and IL-17A production was quantified by flow cytometry. (**A**) Fraction of $CD3^+$ and $CD3^-$ cells within the IL-$17A^+$ cell pool ($n = 8$). Representative plots are gated for lymphocytes. (**B**) Indicated immune cell subsets were quantified within the $CD3^+$IL-$17A^+$ cell pool ($n = 15$). (**C**) IL-17A and IFN-γ production by hepatic γδ T cells upon in vitro restimulation with PMA and ionomycin in WT mice after 2 weeks of NCD or SSD feeding ($n = 5$). Representative FACS plots are gated for γδ T cells. The number next to the outlined area represents the percentage of IFN-γ– or IL-17A–producing γδ T cells. (**D**) WT mice were fed an NCD or an SSD diet for 2 weeks and liver resident γδ T cells were analyzed by flow cytometry for expression of transcription factors T-Bet, RORγt and Eomesodermin (Eomes) ($n = 5$). (**E**) CD3ε staining of *Tcra*$^{-/-}$ mice after 2 weeks of feeding with NCD or SSD. Scale bars, 100 μm. (**F**) WT mice were fed an NCD or SSD for 2 weeks and for the last 4 days given BrdU in drinking water. Tissue-resident cells were visualized by injecting animals with biotinylated CD45 5 min before isolation of livers, followed by fluorescent labeling using streptavidin-eFluor780 and analysis by flow cytometry. Tissue-resident cells were defined as eFluor-780$^-$. $Ki67^+$ and $BrdU^+$ hepatic γδ T cells were quantified by flow cytometry ($n = 5$). (**G**) Quantification of NKG2D expression on hepatic γδ T cells by flow cytometry of mice fed 2 weeks with an NCD or SSD ($n = 14$). The representative plot shows γδ T cells after PMA/ionomycin stimulation. (H and I) Mice were fed an SSD for 2 weeks. Hepatic γδ T cells were restimulated in vitro, and IL-17A production was determined by flow cytometry. (**H**) IL-17A production of γδ T cells after stimulation with αCD3, plate-bound αNKG2D, or their combination, measured by flow cytometry. (**I**) Relative increase of IL-17A production within hepatic γδ T cells from WT or *Klrk1*$^{-/-}$ mice upon in vitro restimulation with αCD3 alone or in combination with plate-bound αNKG2D over nonstimulated γδ T cells ($n = 5$). Representative FACS plots are gated for γδ T cells. Numbers show percentages of IL-17A–producing γδ T cells (**J**) WT and Klrk1$^{-/-}$ mice were fed an SSD for 2 weeks. Hepatic γδ T cells were restimulated in vitro with PMA/ionomycin, and IL-17A production was measured by flow cytometry. Shown is the relative increase in IL-17A production within SSD-fed over NCD-fed mice ($n = 5$ to 6). The data are representative of at least two independent experiments. Shown are means ± SEM. Statistical significance was determined by unpaired *t* test (A to G), paired *t* test (H and I), and ANOVA with Bonferoni post-testing (J). Statistical significance was defined as $^*P < 0.05$, $^{**}P < 0.01$, and $^{***}P < 0.001$.

of IL-17A in our model, suggesting that γδ T, and, to a lesser extent, $CD4^{-}CD8^{-}$ T cells play a dominant role in the induction of NKG2D-mediated fibrosis after SSD feeding.

γδ T cells increased after SSD but not HFD feeding and showed the strongest increase in IL-17A production (Fig. 6B and fig. S6B). We therefore decided to focus on the role of γδ T cells in NKG2D-dependent IL-17A production in the liver. After SSD feeding, hepatic γδ T cells rapidly and potently induced IL-17A production, whereas their ability to produce IFN-γ, TNF, IL-17F, and IL-22 was not affected (Fig. 6C and fig. S6, C and D). In accordance with this cytokine profile, γδ T cells induced the expression of the transcription factors RORγt and Eomesodermin, whereas there was a relative reduction in the percentage of cells expressing T-bet (Fig. 6D). Multidimensional analysis of γδ T cell populations by *t*-distributed stochastic neighbor embedding revealed that animals fed with an NCD contained a relatively homogenous population with regard to CD44 and CD27 expression. In contrast, SSD feeding induced polarization of γδ T cells toward an $IL\text{-}17A^{+}CD27^{-}CD44^{Bright}$ profile (fig. S6E), a phenotype typically associated with IL-17A–producing γδ T cells ($γδ^{17}$ T cells) (*39*). Moreover, in SSD-fed mice, IL-17A was predominantly produced by $Vγ6^{+}$ cells and was associated with a relative decrease in the frequency of $Vγ1^{+}$ cells within the γδ T cell pool compared with NCD-fed controls (fig. S6F).

To confirm that $γδ^{17}$ T cells play a general role in development of NASH pathology and not just in the SSD model, animals were fed a methionine and choline–deficient diet (MCD). This model induces liver steatosis and fibrosis after 12 weeks of feeding because of an inability of hepatocytes to form very low density lipoproteins, although it causes weight loss rather than weight gain in animals (*40*). WT and $Tcrd^{-/-}$ mice were placed on an MCD, and immune cells and liver pathology were analyzed after 12 weeks. MCD caused an increase in γδ T cells in livers of WT animals, which was comparable to that observed after SSD feeding (fig. S6G). γδ T cells significantly increased IL-17A production ($P = 0.0012$) and became the dominant source of this cytokine in the liver (fig. S6, H and I). MCD-fed $Tcrd^{-/-}$ mice had reduced pathology compared with WT controls, because they lost significantly less weight ($P = 0.0005$) (fig. S6J). In addition, liver fibrosis was considerably lower in $Tcrd^{-/-}$ mice (fig. S6K).

Previously, a lipid-rich environment was shown to promote the specific outgrowth of $γδ^{17}$ T cells, because these cells preferentially use oxidative phosphorylation to fulfill their energetic needs (*41*). We therefore hypothesized that the increase of γδ T cells in steatotic livers was the result of local proliferation. We observed that γδ T cells predominantly resided in the parenchyma of the liver and not in the sinusoids, both after NCD and SSD feeding (Fig. 6E). In vivo labeling of $CD45^{+}$ cells in the circulation of SSD-fed mice confirmed that a larger fraction of γδ T cells was tissue resident in the liver than αβ T cells, explaining why the former population more vigorously responds to NKG2D-Ls expressed on hepatocytes (fig. S6L). To exclude increased influx from the periphery as a reason for γδ T cell increase, we isolated leukocytes from the livers of animals 2 weeks after initiation of SSD feeding and injected them into NCD– or SSD–co-fed animals. We did not observe a difference in the number of either αβ or γδ donor T cells infiltrating the spleen or liver of NCD- or SSD-fed mice (fig. S6M). We therefore analyzed proliferation of hepatic, tissue-resident γδ T cells in response to 2 weeks of SSD feeding and found that their expression of Ki67 was significantly increased ($P = 0.0088$) (Fig. 6F). In addition, SSD-fed animals pulsed with 5-bromo-2′-deoxyuridine (BrdU) showed a significant increase of its incorporation in hepatic γδ T cells (Fig. 6F). Cells expressing NKG2D and RORγT proliferated faster than γδ T cells not expressing these proteins as shown by Ki67 staining (fig. S6, N and O). These results suggest that the increase of $NKG2D^{+}$ $γδ^{17}$ T cells in livers of SSD-fed mice is due to preferential outgrowth of tissue-resident cells rather than ingress from the periphery.

Last, we wanted to determine whether NKG2D stimulation of hepatic γδ T cells promotes their production of IL-17A. We found that nearly all γδ T cells that produce IL-17A also express NKG2D on their surface. Moreover, the total fraction of NKG2D-expressing γδ T cells in the liver significantly increased in response to SSD feeding (Fig. 6G). Next, we stimulated γδ T cells in vitro with agonistic antibodies against NKG2D, CD3ε, or both simultaneously. We observed that NKG2D only promoted IL-17A production when stimulated in concert with the TCR (Fig. 6, H and I). This synergistic effect was not observed in γδ T cells derived from $Klrk1^{-/-}$ mice, indicating that NKG2D potentiates a TCR-mediated signal to drive cytokine production (Fig. 6I). To confirm these observations in vivo, WT and $Klrk1^{-/-}$ mice were placed on an NCD or SSD for 2 weeks, and IL-17A production was measured after in vitro restimulation of hepatic γδ T cells with PMA/ionomycin. Whereas WT cells showed a strong increase in the number of γδ T cells producing IL-17A upon SSD feeding, $Klrk1^{-/-}$ mice showed no differences in cytokine output (Fig. 6J). The absolute number of γδ T cells in the liver was not affected by NKG2D deficiency (fig. S6P). Thus, NKG2D stimulates IL-17A production by tissue-resident γδ T cells in the context of MAFLD.

NKG2D signaling drives inflammation in the context of NASH

To gain more insight into the inflammatory processes mediated by NKG2D during development of NASH, we first analyzed the kinetics of hepatic immune cell populations in response to SSD feeding. We noticed that the NASH-inducing diet caused an increase of immune cells in three waves. Within 2 weeks after initiating feeding, NK cells and γδ T cells increased and remained higher during the entire 16-week period of feeding (Fig. 7A). The numbers of NKT cells remained comparable between SSD- and NCD-fed mice in the entire experiment. About 4 weeks after the initiation of feeding, we observed a second wave of immune cells infiltrating the liver, dominated by $F4/80^{Bright}$, proinflammatory macrophages, and, to a lesser extent, neutrophils and eosinophils (Fig. 7A). Third, at around 8 weeks of feeding, $CD8^{+}$ T cell numbers increased, which agrees with other murine models for NASH (*4*). $CD4^{+}$ T cell and B cell populations remained mostly unaffected by SSD feeding (Fig. 7A). These findings suggest that SSD-induced liver inflammation is initiated by a wave of innate-like lymphocytes, which drives recruitment of myeloid cells and ultimately promotes the accumulation of CD8 T cells.

Our RNA-sequencing data indicated that IL-17A promotes chemokine production by liver cells (Fig. 5C), which may explain how innate-like lymphocytes initiate the second wave of myeloid cells. To confirm this finding, primary hepatocytes were stimulated in vitro with IL-17A, and chemokine expression was determined by quantitative polymerase chain reaction (qPCR). We observed that in response to stimulation, hepatocytes induced expression of the chemokines CXCL1 and CXCL2 and, to a lesser extent, CCL2

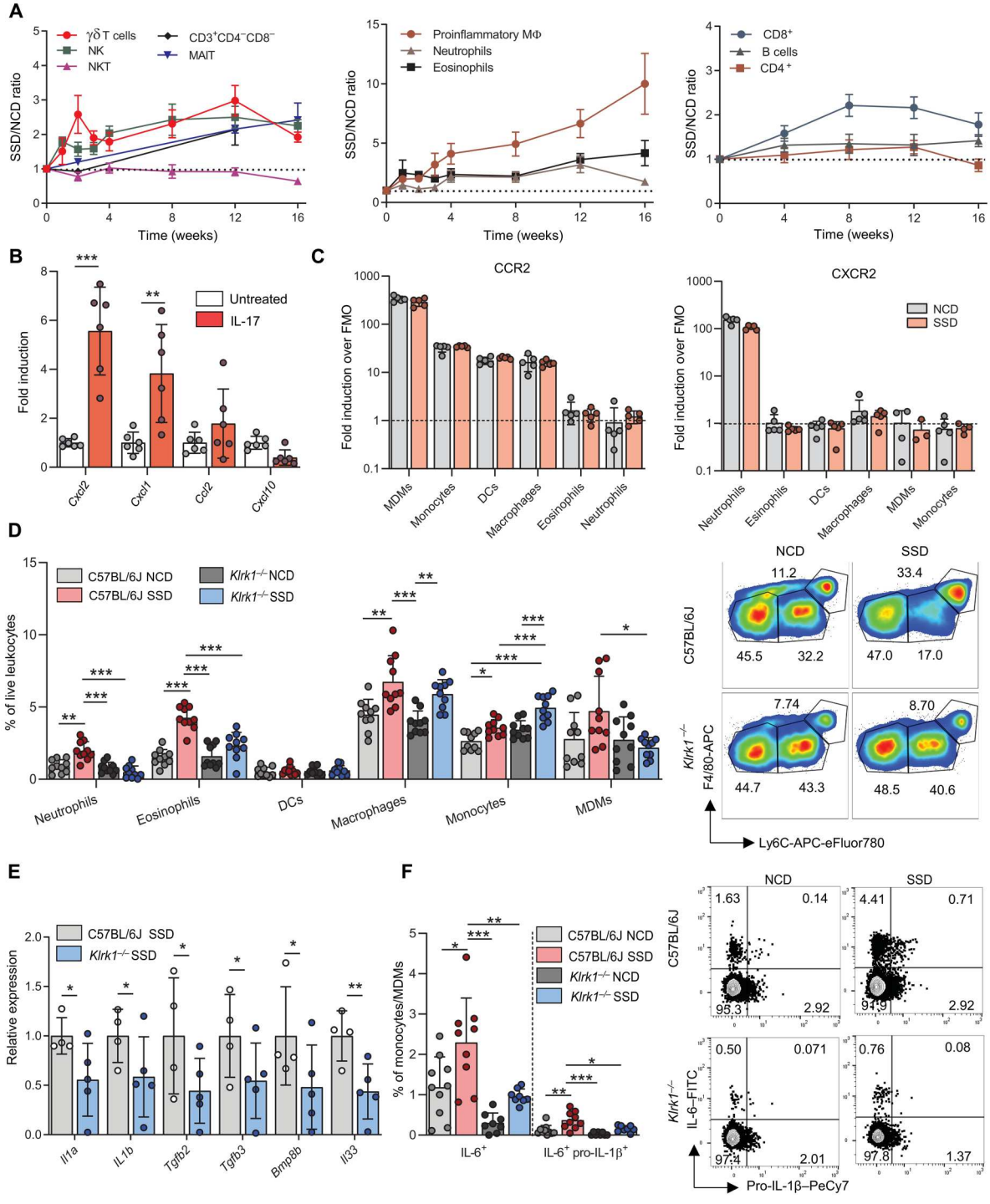

Fig. 7. NKG2D mediates myeloid cell recruitment in the context of NASH. (**A**) WT mice were fed with an NCD or SSD, and at the indicated times hepatic immune cell numbers were quantified by flow cytometry ($n = 6$ to 10). (**B**) Primary hepatocytes were cultured with or without IL-17A, and expression of indicated chemokines was determined by qPCR ($n = 6$). (**C**) WT mice were fed an NCD or SSD for 4 weeks, and the levels of CCR2 and CXCR2 expression on indicated myeloid cell populations were measured by flow cytometry. (**D**) WT and *Klrk1*$^{-/-}$ mice were fed for 4 weeks with an NCD or SSD. Hepatic leukocytes of the myeloid lineage were quantified by flow cytometry ($n = 10$). Representative plots are gated for CD11b^{+}F4/80^{+} cells. (**E**) WT and *Klrk1* $^{-/-}$ mice were fed an SSD for 3 weeks, and the total transcriptome of liver tissue was analyzed by RNA sequencing. Expression of indicated genes associated with inflammation ($n = 3$ to 5). (**F**) WT and *Klrk1*$^{-/-}$ mice were fed an SSD for 4 weeks, and hepatic leukocytes were restimulated in vitro with PMA/ionomycin for 4 hours. Production of indicated cytokines was measured by flow cytometry ($n = 9$ or 10). Representative FACS plots are gated for monocyte/MDM populations. Numbers represent the percentage of cytokine-producing cells. The data are representative of one experiment using three to five biological replicates (E), two pooled experiments (B, D, and F) or at least two independent experiments (A and C). Shown are means ± SEM. Statistical significance was determined by ANOVA with Bonferoni posttesting (D and F) or by unpaired t test (A, C, and E). Statistical significance was defined as $^{*}P < 0.05$, $^{**}P < 0.01$, and $^{***}P < 0.001$. DCs, dendritic cells.

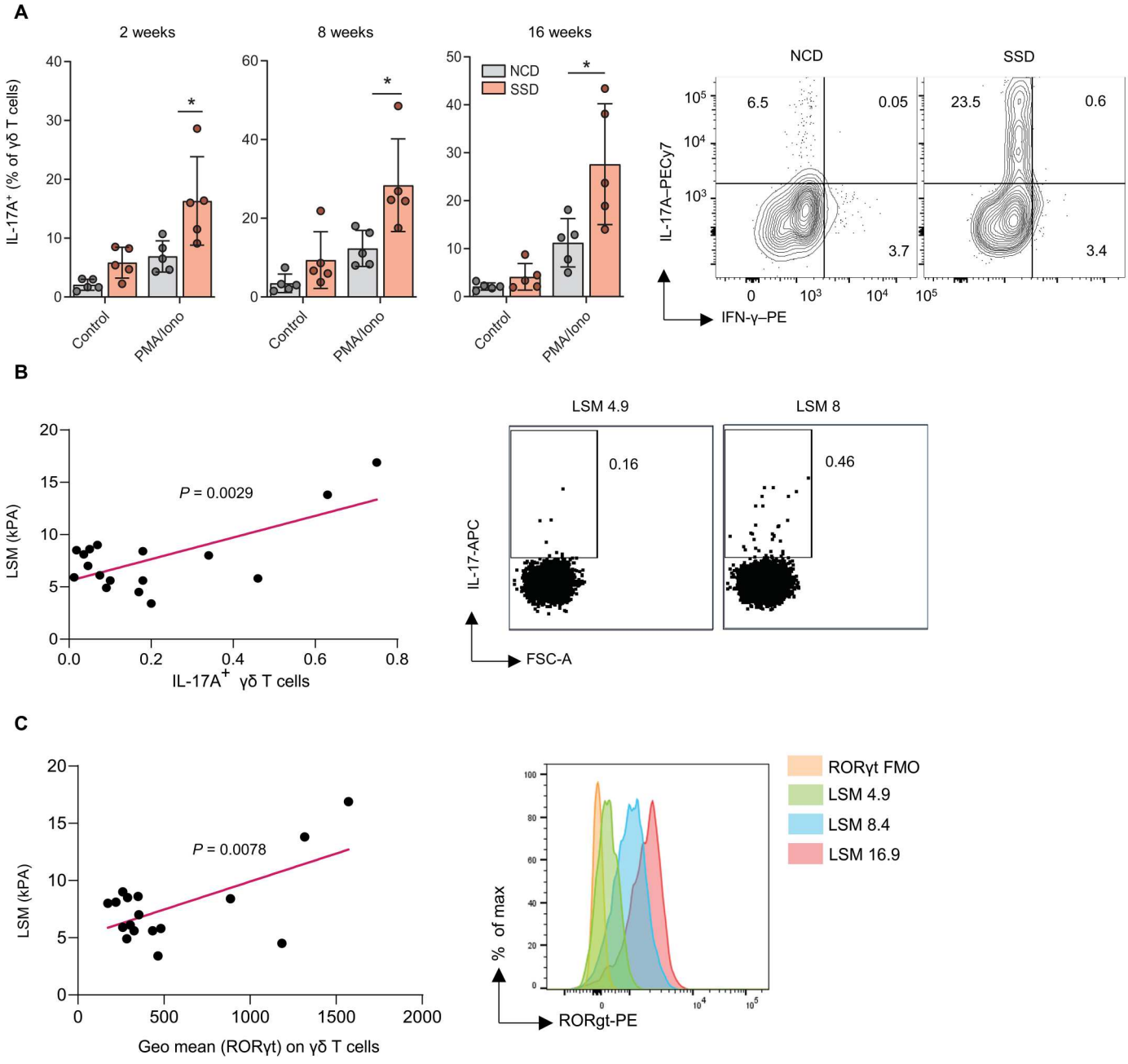

Fig. 8. IL-17A$^+$Roryt$^+$ γδ T cells in blood are a potential noninvasive biomarker for human NASH. (**A**) WT mice were fed with an NCD or SSD diet. At indicated time points, blood leukocytes were restimulated in vitro with PMA/ionomycin, and IL-17A production by γδ T cells was measured by flow cytometry ($n = 5$). (**B** and **C**) Human patients with MAFLD were analyzed for liver stiffness (LSM) by US measurement. Next, their PBMCs were restimulated in vitro with PMA/ionomycin, and γδ T cells were analyzed by flow cytometry. (**B**) Correlation between LSM (an indicator of fibrosis) and IL-17A production by γδ T cells ($n = 18$). (**C**) Correlation between LSM and RORγt expression by γδ T cells ($n = 18$). Shown are means ± SEM. Statistical significance was determined by unpaired *t* test (A) or by linear regression (B and C). Statistical significance was defined as $^*P < 0.05$, $^{**}P < 0.01$, and $^{***}P < 0.001$.

(Fig. 7B), which are potent recruiters of proinflammatory cells of the myeloid lineage (*42*). CXCR2 is the receptor for CXCL1 and CXCL2, whereas CCR2 is the receptor for CCL2. We observed that CXCR2 was highly expressed on hepatic neutrophils, whereas CCR2 could be detected on monocyte-derived macrophages (MDMs), monocytes, and macrophages, independent of the diet (Fig. 7C). Most lymphocytes did not express either receptor (fig. S7A). In accordance with the expression profile of these two chemokine receptors, we observed that the absolute number and percentage of neutrophils and Ly6C$^+$ monocytes/macrophages increased in response to SSD feeding (Fig. 7D and fig. S7, B to D). The increase of most of these populations in response to SSD feeding was considerably less in animals deficient for NKG2D (Fig. 7D and fig. S7, C and D).

Last, we analyzed whether the inflammatory environment was affected by NKG2D deficiency. Total transcriptome analysis of total liver lysates of WT and *Klrk1*$^{-/-}$ mice after 3 weeks of SSD feeding showed a marked decrease in genes associated with IL-6 regulation (fig. S7E), a cytokine that has been associated extensively with NASH (*43*). In addition, gene expression of several proinflammatory cytokines associated with NASH, including IL-1β, were notably reduced in the livers of SSD-fed *Klrk1*$^{-/-}$ animals compared with WT controls (Fig. 7E). We therefore analyzed whether NKG2D deficiency affected production of these proinflammatory cytokines. SSD feeding resulted in a substantial increase of both IL-6 and IL-1β production by monocytes and MDMs. Production of these cytokines was appreciably reduced in animals deficient for NKG2D (Fig. 7F and fig. S7E). In summary, NKG2D signaling is required for liver inflammation in the context of MAFLD and promotes proinflammatory cytokine production by myeloid cells.

IL-17A^{+}Rorγt^{+} γδ T cells in blood are a noninvasive biomarker for human MAFLD

Few reliable biomarkers for NASH are currently available, especially during the early phases of the disease. The gold standard for diagnosis is a liver biopsy, which is an invasive procedure with a high chance of complications (*2*). We wanted to investigate whether changes in the immunological profile of hepatic immune cells associated with NASH can be detected in the blood. Mice were placed on an SSD, and IL-17A production by γδ T cells isolated from the blood was determined after in vitro restimulation. We observed a significant increase in IL-17A–producing γδ T cells in the blood 2 weeks after initiation of feeding ($P = 0.0296$), which closely mirrored their phenotype in the liver (Fig. 8A and fig. S8A). In contrast, IFN-γ and TNF production were not affected in these cells (fig. S8A). The increased IL-17A production by γδ T cells in the blood was retained over a period of 16 weeks of SSD feeding (Fig. 8A), indicating that it is a potential marker for metabolic stress in the liver in the context of NASH.

To determine whether a similar profile could be detected in humans, blood was isolated from patients in whom MAFLD was confirmed by ultrasound (US) techniques. We observed a marked increase in IL-17A production by blood γδ T cells. This value positively correlated with the severity of liver stiffness [liver stiffness measurement (LSM); Fig. 8B], which is a surrogate marker of fibrosis (*44*). A similar correlation was observed between liver stiffness and γδ T cells expressing the transcription factor Rorγt (Fig. 8C). In contrast, LSM did not correlate with either the total frequency of γδ T cells or with the frequency of T_H17 cells and IL-17A–producing MAIT cells in the blood of patients (fig. S8, B and C). Although they are not the dominant source of cytokines in circulation, these findings indicate that IL-17A production by γδ T cells best represents the inflammatory status of liver inflammation measurable in blood and has the potential to be a reliable noninvasive biomarker for NASH in humans.

In summary, metabolic stress of liver cells is sensed by tissue-resident ILTs such as γδ T cells through the NKG2D receptor. In response, they produce IL-17A, which licenses hepatocytes to produce chemokines that recruit proinflammatory cells and mediate inflammation and fibrosis (fig. S8D).

DISCUSSION

MAFLD affects about one-quarter of the global adult population, yet its impact on public health has long remained unrecognized (*45*). The transition of MAFL to NASH marks the initiation of a process that may lead to fibrosis, loss of liver function, and death (*2*). Elucidation of how this process is mediated is therefore of great clinical importance. Here, we found that hepatocytes up-regulate surface expression of NKG2D-Ls after lipid accumulation. This signal of metabolic stress is detected by tissue-resident ILTs and drives their production of IL-17A. Hepatocytes are licensed directly by IL-17A to produce chemokines that recruit proinflammatory cells into the liver, leading to development of NASH and fibrosis. Deficiency of NKG2D, γδ T cells, or the IL-17A receptor on hepatocytes could prevent inflammation and fibrosis while not affecting steatosis.

The transition of MAFL to NASH was proposed to require multiple instigators, such as oxidative stress, fat accumulation, and a microbiome imbalance (*2*). How these factors are translated into a signal that activates the immune system was unclear. Previously, microbiota-derived lipid antigens were shown to be important for MAFLD-induced expansion of γδ T cells in the liver, yet how these cells were subsequently activated was unclear (*11*, *13*). Our findings indicate that lipid accumulation, most notably of cholesterol, leads to induction of NKG2D-Ls and activation of γδ T cells. How cholesterol drives metabolic stress is unknown but may involve liver X receptors (LXRs). LXRs are transcription factors that are activated in response to high cholesterol levels and mediate oxysterol metabolism (*46*). Agonists of these receptors were shown to induce expression of the NKG2D-Ls MICA and MICB in human cells (*46*). Reverse agonists of LXRs have a beneficial impact on systemic lipid metabolism and liver pathology in context of MAFLD, and several of these compounds have been tested in clinical trials (*47*, *48*). We cannot exclude that SSD feeding mediates activation of immune cells at other sites such as adipose tissue, which was shown to mediate IL-17A production in tissue-resident γδ T cells (*37*). Nevertheless, our finding that IL-17A receptor deficiency on hepatocytes does ameliorate pathology suggests that this cytokine primarily mediates its effect on the liver.

A hallmark of MAFLD is the formation of IL-17A–mediated type 3 inflammation, which is a driving force behind the pathogenesis of NASH and HCC (*7*, *12*, *49*–*53*). A recent study showed that the steatotic liver microenvironment gives rise to proinflammatory CXCR3^{+} T_H17 cells, which produce elevated levels of IL-17A and TNFα (*54*). However, T_H17 cells are typically only formed later during the immune response, and the signal that initiates immune polarization in MAFLD was left unexplored. Our findings indicate that in MAFLD, NKG2D-Ls are the primary signal that communicates loss of tissue homeostasis to intraparenchymal ILTs, which produce IL-17A to initiate type 3 inflammation. IL-17A predominantly targets nonhematopoietic cells, including hepatocytes (*42*, *55*). IL-17A receptor deficiency on hepatocytes did not protect animals from developing fibrosis to the extent seen in *Klrk1*$^{-/-}$ mice, suggesting that additional factors are induced by NKG2D engagement. Recently, granulocyte-macrophage colony-stimulating factor (GM-CSF) was shown to be important for development of fibrosis in animal models of NASH, and γδ T cells can produce high levels of this cytokine (*12*, *56*). Whether γδ T cell–derived GM-CSF is also important for development of SSD-

induced liver fibrosis is currently unclear. Nevertheless, production of chemokines that attract myeloid cells to the infected or injured site is the hallmark of IL-17A signaling (*42*, *57*). Deficiency of this cytokine or its signaling components results in decreased hepatic accumulation of myeloid cells in models of NASH (*6*, *51*). Our findings indicate that NKG2D-induced IL-17A production directly licenses hepatocytes to produce CXCL1, CXCL2, and CCL2, which were previously shown to be crucial for neutrophil accumulation, HSC activation, and fibrosis in NASH (*58*, *59*). Thus, our study elucidates the first step in metabolic stress–induced type 3 liver inflammation.

NKG2D is classically associated with type I immune responses against viruses and tumors, whereas we now show that this receptor drives IL-17A production. NKG2D is expressed on NK cells and antigen-experienced CD8 T cells and NKT cells, and their engagement of its ligands leads to the production of IFN-γ, an archetype T_H1 cytokine (*19*, *20*, *35*). These immune cells are also present in the liver, and it was therefore unexpected that NKG2D-L induction by hepatocytes only activates a subset of ILTs specialized in the production of IL-17A. However, T_H1- and T_H17-type NKG2D$^+$ immune cells are found at different sites in the liver. NK cells and NKT cells are predominantly present in the liver sinusoids and will therefore most efficiently respond to incursions such as viral infections, which target the endothelium of the liver blood vessels and cells located within the space of Diss (*60*). Our findings indicate that hepatic γδ T cells are present in the parenchyma of the liver and are therefore the first responder to signals coming from hepatocytes. Also, in human tissues, most IL-17A$^+$ cells of patients with NASH appeared to be in direct contact with hepatocytes. Thus, the location of NKG2D-Ls appears crucial for the way in which the consequent immune response polarizes.

In summary, our study identifies a key mechanism for the transition from MAFL to NASH in patients with metabolic liver disease and has great potential as a therapeutic target for the treatment of MAFLD. In addition, the frequency of IL-17$^+$RORγt$^+$ γδ T cells in the blood of patients with MAFLD positively correlated with US-based techniques for the quantification of fibrosis. Measurement of these cells in people with MAFLD therefore has great potential as a noninvasive marker for the diagnosis of NASH.

MATERIALS AND METHODS

Study design

The goal of this study was to identify the mechanism via which hepatocytes communicate metabolic stress to the immune system and initiate the inflammation that marks the transition of MAFL to NASH. To this end, we generated a new dietary model to induce NASH in mice and analyzed changes in immune cell subsets after feeding. Sample size was determined by a power analysis based on previous experiments pilot studies. We assumed a power of 85%, a within-group variation of 20 to 30%, and a between-group difference of 50 to 100%. A 95% confidence interval was considered statistically significant. Dependent on the parameter, group sizes per experiment were four to eight animals. A similar power analysis was performed for experiments using human samples, which dictated the use of at least 16 samples. All data that were collected were also included in the analysis. Each experiment was performed at least twice under the same conditions. Experiments were blinded as much as possible through assignment of groups by people that were not further involved in the experiments.

Patients

Patients were included at the NAFLD polyclinics at KBC Rijeka. All patients were over 18 years of age and signed an informed consent before inclusion. All patients were subjected to laboratory analysis, abdominal US, and transient elastography (TE) measurements using a FibroScan 502 Touch (Echosense, Paris, France). Patients with incomplete data; those who refused to undergo TE or US examination; those with frequent alcohol consumption (>20 g per day for men and >10 g per day for women), other chronic liver diseases (viral, metabolic, or autoimmune), or celiac disease; and those with secondary causes of fatty liver such as drugs (amiodarone and tamoxifen) were excluded from the final analysis. In addition, active malignancy, congestive heart failure and valvular heart disease, TE failure, and pregnancy were additional exclusion criteria.

In all patients, TE examination after overnight fasting was done by FibroScan, which was performed using M or XL probe by an experienced gastroenterologist. The examination was defined as valid if there were ≥10 valid measurements with interquartile range–to–median ratio of LSM ≤ 0.3. The diagnosis of liver steatosis was considered in patients with CAP ≥ 238 dB/m (*61*). Patients with LSM ≥ 7 kPa were defined to have a high liver fibrosis (≥F2), whereas an advanced fibrosis (≥F3) was considered if LSM was ≥9.6 kPa using the M probe or ≥9.3 kPa using the XL probe. Last, patients with LSM ≥ 11.5 kPa using the M probe or ≥ 11.0 kPa using XL probe were defined as having cirrhosis. Cutoff values were previously defined (*62*, *63*). US-guided liver biopsies were done by an experienced gastroenterologist.

The Clinical Hospital Rijeka Ethics committee approved this research under number 003-05/15-2/60. Fresh biopsy material was obtained by the Department of Pathology and Molecular Pathology, University Hospital Zurich and was approved by the local ethics committee (Kantonale Ethikkommission Zürich, KEK-ZH-No. 2013-0503). We conducted the research in accordance and agreement with the International Conference on Harmonization guidelines on Good Clinical Practice and with the Declaration of Helsinki.

Mice

Mice were strictly age and sex matched within experiments, held under specific pathogen–free conditions, and handled in accordance with institutional, national, and/or EU guidelines. Male mice (8 to 12 weeks old) were fed ad libitum with an NCD (SSNIFF) or an SSD enriched in fat [40% of calories derived from animal fat (Bregi) and fructose (22% (SSNIFF)] and cholesterol [2% (SSNIFF)]. Where indicated, mice were fed with either HFD, where 50% of calories were derived from pig fat (Bregi); HCD containing 2% of cholesterol (SSNIFF); or MCD purchased from SSNIFF. All lines were kept as breeding colonies in the local animal facility in Rijeka, Croatia, under specific pathogen–free conditions. All animal experiments were done with approval from the University of Rijeka Medical Faculty Ethics Committee and Croatian Ministry of Agriculture, Veterinary and Food Safety Directorate, under number UP/I-322-01/21-01/31.

Cell isolation

Mice were euthanized by O_2/CO_2 intoxication followed by CO_2 suffocation and perfused with phosphate-buffered saline (PBS). Livers were collected and directly smashed through sieve or first cut into small pieces and digested with collagenase IV (1 mg/ml; Sigma-Aldrich) and deoxyribonuclease (2 mg/ml) in Hank′s balanced salt solution (HBSS; with Ca^{2+}/Mg^{2+}) supplemented with 5% fetal bovine serum (Sigma-Aldrich). The cell suspension was centrifuged (500*g* for 5 min). The leukocytes in the pellets were isolated by gradient centrifugation with 40 and 80% Percoll. Cells were collected, washed with RPMI, and centrifuged. Pellet was incubated for 3 min in ACK (ammonium-chloride-potassium; Sigma-Aldrich) buffer to lyse erythrocytes and resuspended in 3% RPMI. Spleens were first passed through a 70-μm cell strainer, washed with 3% RPMI, and centrifuged. Blood was collected into an EDTA-containing tail vein, and peripheral blood mononuclear cells (PBMCs) were isolated with Lymphoprep (Serumwerk Bernburg) gradient centrifugation. Hepatocytes used for subsequent fluorescence-activated cell sorting (FACS) analysis were isolated by collagenase I perfusion in situ through the portal vein and subsequent homogenization on magnetic stirrer. For the establishment of cultured primary hepatocytes, livers were processed by the step collagenase perfusion as previously described (*64*). In brief, mice were anesthetized with ketamine/xylazine (Vetoquinol). Upon cannulation, mice were perfused via inferior vena cava with prewarmed perfusion buffer [HBSS (Sigma-Aldrich) supplemented with 25 mM Hepes (Sigma-Aldrich) and 0.5 mM EDTA (VWR Life Sciences)] until bleaching of the liver was achieved. Next, the perfusion buffer was omitted for digestion buffer [HBSS with 25 mM Hepes and Liberase Research Grade (25 μg/ml; Sigma-Aldrich)]. In situ digestion was followed by the digestion in the petri dish with Williams E medium (PAN Biotech). The liver sack was ruptured with forceps along the surface, and cells were released using a cell scraper and then strained through a sieve. Separation of live primary hepatocytes was achieved by centrifugation in Percoll. Pellet was resuspended in Williams E medium and plated in six-well plates. Primary murine hepatocytes were stimulated by either 200 μmol of oleic acid (Sigma-Aldrich), cholesterol (200 μg/ml; SSNIFF), 25 mM fructose (SSNIFF), and/or IL-17A (25 μg/ml; PreproTech) in 10% Williams E medium. Cells were treated for 48 hours and analyzed by qPCR or confocal microscopy. Human PBMCs were isolated from peripheral blood by density gradient centrifugation using Histopaque 1077 Density Gradient Medium (Sigma-Aldrich, St. Louis, USA).

Flow cytometry

Cells were stained and analyzed in PBS containing 1% bovine serum albumin (BSA) and NaN_3 and pretreated with Fc block (clone 2.4G2, produced in-house at the University of Rijeka). Fixable viability dye eFluor 780 (eBioscience) was used to exclude dead cells. For intracellular staining, cells were stimulated for 4 hours in vitro with PMA and ionomycin (Sigma-Aldrich) supplemented with brefeldin A (eBioscience) or GolgiPlug and GolgiStop (both 1:1000; BD Biosciences). For specific stimulation of γδ T cells through receptors, 96-well microtiter plates were precoated with αNKG2D (MI-6) and 145-2C11 hybridoma supernatant containing αCD3 was added in the stimulation mixture containing brefeldin A and αCD3-PE-eFluor 610. Permeabilization and fixation of cells was done with the Fix/Perm kit (BD Biosciences). Bodipy$^{493/503}$ (BD) staining was used according to manufacturer′s protocol to assess relative lipid content in cells. Staining of nuclear proteins (T-bet, eomes, and ROR-γt) was done with the FoxP3 staining buffer set (eBioscience). BrdU labeling and staining were performed according to the BrdU flow kit instructions (BD Biosciences). Most flow cytometry experiments were done on a FACSverse or FACSaria (BD Biosciences) or MACS Quant Analyzer 16 (Mitenyi Biotec). Human liver leukocytes were measured on 5L Cytek Aurora (Cytek). Dead cells and doublets were excluded from the analysis using SSC-A/H, FSC-A/H, and a fixable viability kit (LIVE/DEAD Blue, Thermo Fisher Scientific). FCS files were analyzed using FlowJo (TriStar) software.

Histology

For immunohistology, tissues were fixed in 4% formalin for at least 48 hours, dehydrated, and paraffin embedded. Sections (2 μm) were cut and deparaffinized, and antigen retrieval was performed by using 1 M sodium citrate buffer or a tris-EDTA (pH = 9) buffer. Sections were blocked with goat serum and then incubated with primary antibodies overnight at 4°C. After endogenous peroxidase block using 0.3% H_2O_2, slides were incubated for 1 hour with secondary antibody. Staining was visualized with DAB (Dako) and brief hematoxylin counterstaining. Collagen deposition was detected with Sirius red staining on deparaffinized slides stained with a 0.1% Picro-Sirius red solution (Sigma-Aldrich, USA) for 1 hour. Slides were washed in acidified water, dehydrated, and mounted with Entellan (Sigma-Aldrich, USA). Basic structural parameters were observed on slides stained with hematoxylin and eosin. Stainings were quantified using ImageJ software [National Institutes of Health (NIH)] or by scoring of blinded samples by an expert pathologist according to established definitions (*65*). Immunopathology was quantified by adding the scores of infiltration foci, cysts, and granulomas per vision field (200× magnification). For immunofluorescence, liver slides were deparaffinized, and antigen retrieval was performed using tris-EDTA buffer. Sections were blocked with 3% BSA for 1 hour at room temperature. Subsequently, sections were incubated overnight with primary antibodies [Ki67 (Invitrogen) and CD45 (Cell Signaling)]. Secondary antibodies were incubated for 1 hour at room temperature (RT), nuclei were counterstained with 5′ 4′,6-diamidino-2-phenylindole incubation, and slides were mounted with Mowiol 4-88. For confocal microscopy, primary murine hepatocytes were fixed in 4% paraformaldehyde (PFA) for 15 min at RT. Cells were washed twice with PBS and permeabilized for 5 min using 0.1% Triton-X 100. Cells were washed two times with PBS and incubated with Bodipy$^{493/503}$ (1.25 μg/ml; BD Bioscience) for 30 min. Cells were washed twice with PBS and analyzed at RT with a Leica TCS SP8 confocal laser scanning microscope using an HC PL APO 40×/1.30 OIL CS2 objective and LasX acquisition software (version 3.5.6.21594) without gamma adjustments.

Quantitative PCR

RNA was isolated from primary murine hepatocytes using NucleoZOL (MACHEREY-NAGEL) according to the manufacturer′s protocol, and complementary DNA was generated with a reverse transcription core kit (Eurogentec). The expression of mRNA was examined by quantitative PCR with a 7500 Fast Real Time PCR machine (ABI). The relative mRNA expression was normalized by quantification of hypoxanthine-guanine phosphoribosyltransferase (HPRT) housekeeping gene in each sample.

RNA sequencing

Total RNA of liver samples was extracted using the Qiagen RNeasy Micro Kit according to the manufacturers' protocol. Sequencing of 100-bp single reads was done on Illumina Novaseq 6000 (Illumina Inc., CA, USA) at the Functional Genomics Center Zurich. The library was prepared with the Illumina Truseq Total RNA protocol. The resulting raw reads were evaluated for their quality by using FastQC and subsequently mapped to the mouse genome build GRCm39 using STAR aligner. FeatureCounts was used to quantify the read counts per gene based on GENCODE gene annotation version M26. Differences in gene expression levels between sample groups of interest were calculated as log2 fold changes using DESeq2, and genes exhibiting a false discovery rate–adjusted P value <0.05 and absolute fold changes > 1.5 were considered significant. Hypergeometric overrepresentation analysis based on gene ontology was applied to log-transformed and normalized counts using the clusterProfiler package. RNA-sequencing data were deposited at the Gene Expression Omnibus database of National Center for Biotechnology Information under identifier GSE200482.

ELISA

Serum samples were obtained from NCD- and SSD-fed mice, and concentrations of HMGB1 protein were determined by commercial HMGB1 enzyme-linked immunosorbent assay (ELISA) colorimetric kit (Novus Biologicals) according to the manufacturer's protocol. Plates were analyzed using a Mithras LB940 ELISA plate reader (Berthold Technologies).

In vivo experiments

VATectomy was done as previously described (*27*). Briefly, mice either underwent sham operation or had peri-epididymal fat pad removed (VATectomy). After 2 weeks, mice were placed on an NCD or an SSD diet for 16 weeks. For adoptive transfers, WT (CD45.2) mice were NCD or SSD fed. After 14 days, animals were injected intravenously with 5×10^5 hepatic lymphocytes from NCD (CD45.1)– and SSD (CD45.1/2)–co-fed animals, mixed in a 1:1 ratio. Twenty-four hours after transfer, the ratio of donor cells in liver and spleen were determined by flow cytometry. For homing experiments, WT (CD45.1) mice were NCD or SSD fed for 2 weeks and injected intravenously with 5×10^5 hepatic leukocytes from WT (CD45.1/2) and *Klrk1*$^{-/-}$ (CD45.2) SSD–co-fed animals, mixed in a 1:1 ratio. After 24 hours, the ratio between WT and *Klrk1*$^{-/-}$ CD3$^+$TCRδ$^+$ and CD3$^+$TCRδ$^-$ cells was determined in spleens and livers by flow cytometry. For NK1.1 depletion experiment, mice were weekly treated with intraperitoneal injection of InVivoMAb anti-mouse NK1.1 (clone PK136). After 16 weeks of NCD and SSD feeding, PBS-injected control mice and anti-mouse NK1.1–treated mice were euthanized, and fibrosis/steatosis was determined as previously described. Labeling of circulating γδ T cells was performed using the intravenous injection of biotin-labeled anti-mouse CD45 antibody (clone 30-F11) (2 μg per mice). Mice were euthanized 5 min after intravenous injection, and livers were perfused and analyzed using flow cytometry as previously described.

Lipidomics

Lipidomic analysis was performed in collaboration with EMBL Metabolomics Core Facility (Heidelberg, Germany). Lipid and fatty acid extraction from blood and livers was performed according to the protocol (PMID: 24820162). Liquid chromatography–tandem mass spectrometry (LC-MS/MS) analysis was performed on a Vanquish UHPLC system coupled to an Orbitrap Exploris 240 high-resolution mass spectrometer (Thermo Fisher Scientific, MA, USA) in negative and positive electrospray ionization mode.

Statistics

Figures represent means and SEM (depicted by error bars). To analyze statistical significance, we used either Student's t test, Mann-Whitney's U test, one-way analysis of variance (ANOVA), with Bonferroni's posttest correction for multiple comparisons, or simple linear regression. P values of <0.05 ($^*P < 0.05$, $^{**}P < 0.01$, and $^{***}P < 0.001$) were considered statistically significant.

Supplementary Materials

This PDF file includes:

Figs. S1 to S8
Table S1

Other Supplementary Material for this manuscript includes the following:

Data files S1 and S2
MDAR Reproducibility Checklist

REFERENCES AND NOTES

1. M. Eslam, P. N. Newsome, S. K. Sarin, Q. M. Anstee, G. Targher, M. Romero-Gomez, S. Zelber-Sagi, V. W.-S. Wong, J.-F. Dufour, J. M. Schattenberg, T. Kawaguchi, M. Arrese, L. Valenti, G. Shiha, C. Tiribelli, H. Yki-Järvinen, J.-G. Fan, H. Grønbæk, Y. Yilmaz, H. Cortez-Pinto, C. P. Oliveira, P. Bedossa, L. A. Adams, M.-H. Zheng, Y. Fouad, W.-K. Chan, N. Mendez-Sanchez, S. H. Ahn, L. Castera, E. Bugianesi, V. Ratziu, J. George, A new definition for metabolic dysfunction-associated fatty liver disease: An international expert consensus statement. *J. Hepatol.* **73**, 202–209 (2020).
2. I. Mikolasevic, S. Milic, T. Turk Wensveen, I. Grgic, I. Jakopcic, D. Stimac, F. Wensveen, L. Orlic, Nonalcoholic fatty liver disease—A multisystem disease? *World J. Gastroenterol.* **22**, 9488–9505 (2016).
3. S. L. Friedman, B. A. Neuschwander-Tetri, M. Rinella, A. J. Sanyal, Mechanisms of NAFLD development and therapeutic strategies. *Nat. Med.* **24**, 908–922 (2018).
4. M. J. Wolf, A. Adili, K. Piotrowitz, Z. Abdullah, Y. Boege, K. Stemmer, M. Ringelhan, N. Simonavicius, M. Egger, D. Wohlleber, A. Lorentzen, C. Einer, S. Schulz, T. Clavel, U. Protzer, C. Thiele, H. Zischka, H. Moch, M. Tschop, A. V. Tumanov, D. Haller, K. Unger, M. Karin, M. Kopf, P. Knolle, A. Weber, M. Heikenwalder, Metabolic activation of intrahepatic CD8$^+$ T cells and NKT cells causes nonalcoholic steatohepatitis and liver cancer via cross-talk with hepatocytes. *Cancer Cell* **26**, 549–564 (2014).
5. M. Dudek, D. Pfister, S. Donakonda, P. Filpe, A. Schneider, M. Laschinger, D. Hartmann, N. Hüser, P. Meiser, F. Bayerl, D. Inverso, J. Wigger, M. Sebode, R. Öllinger, R. Rad, S. Hegenbarth, M. Anton, A. Guillot, A. Bowman, D. Heide, F. Müller, P. Ramadori, V. Leone, C. Garcia-Caceres, T. Gruber, G. Seifert, A. M. Kabat, J.-P. Mallm, S. Reider, M. Effenberger, S. Roth, A. T. Billeter, B. Müller-Stich, E. J. Pearce, F. Koch-Nolte, R. Käser, H. Tilg, R. Thimme, T. Boettler, F. Tacke, J.-F. Dufour, D. Haller, P. J. Murray, R. Heeren, D. Zehn, J. P. Böttcher, M. Heikenwälder, P. A. Knolle, Auto-aggressive CXCR6$^+$ CD8 T cells cause liver immune pathology in NASH. *Nature* **592**, 444–449 (2021).
6. D. A. Giles, M. E. Moreno-Fernandez, T. E. Stankiewicz, M. Cappelletti, S. S. Huppert, Y. Iwakura, C. Dong, S. K. Shanmukhappa, S. Divanovic, Regulation of inflammation by IL-17A and IL-17F modulates non-alcoholic fatty liver disease pathogenesis. *PLOS ONE* **11**, e0149783 (2016).
7. S. Rolla, E. Alchera, C. Imarisio, V. Bardina, G. Valente, P. Cappello, C. Mombello, A. Follenzi, F. Novelli, R. Carini, The balance between IL-17 and IL-22 produced by liver-infiltrating T-helper cells critically controls NASH development in mice. *Clin. Sci.* **130**, 193–203 (2016).
8. M. Rau, A.-K. Schilling, J. Meertens, I. Hering, J. Weiss, C. Jurowich, T. Kudlich, H. M. Hermanns, H. Bantel, N. Beyersdorf, A. Geier, Progression from nonalcoholic fatty liver to nonalcoholic steatohepatitis is marked by a higher frequency of Th17 cells in the liver and an increased Th17/resting regulatory T cell ratio in peripheral blood and in the liver. *J. Immunol.* **196**, 97–105 (2016).

9. M. A. Van Herck, J. Weyler, W. J. Kwanten, E. L. Dirinck, B. Y. De Winter, S. M. Francque, L. Vonghia, The differential roles of T cells in non-alcoholic fatty liver disease and obesity. *Front. Immunol.* **10**, 82 (2019).
10. P. Hegde, E. Weiss, V. Paradis, J. Wan, M. Mabire, S. Sukriti, P.-E. Rautou, M. Albuquerque, O. Picq, A. C. Gupta, G. Ferrere, H. Gilgenkrantz, B. Kiaf, A. Toubal, L. Beaudoin, P. Lettéron, R. Moreau, A. Lehuen, S. Lotersztajn, Mucosal-associated invariant T cells are a profibrogenic immune cell population in the liver. *Nat. Commun.* **9**, 2146 (2018).
11. A. Torres-Hernandez, W. Wang, Y. Nikiforov, K. Tejada, L. Torres, A. Kalabin, S. Adam, J. Wu, L. Lu, R. Chen, A. Lemmer, J. Camargo, M. Hundeyin, B. Diskin, B. Aykut, E. Kurz, J. A. Kochen Rossi, M. Khan, M. Liria, G. Sanchez, N. Wu, W. Su, S. Adams, M. I. U. Haq, M. S. Farooq, V. Vasudevaraja, J. Leinwand, G. Miller, γδ T cells promote steatohepatitis by orchestrating innate and adaptive immune programming. *Hepatology* **71**, 477–494 (2020).
12. T. Fabre, A. M. S. Barron, S. M. Christensen, S. Asano, K. Bound, M. P. Lech, M. H. Wadsworth 2nd, X. Chen, C. Wang, J. Wang, J. McMahon, F. Schlerman, A. White, K. M. Kravarik, A. J. Fisher, L. A. Borthwick, K. M. Hart, N. C. Henderson, T. A. Wynn, K. Dower, Identification of a broadly fibrogenic macrophage subset induced by type 3 inflammation. *Sci. Immunol.* **8**, eadd8945 (2023).
13. F. Li, X. Hao, Y. Chen, L. Bai, X. Gao, Z. Lian, H. Wei, R. Sun, Z. Tian, The microbiota maintain homeostasis of liver-resident γδT-17 cells in a lipid antigen/CD1d-dependent manner. *Nat. Commun.* **7**, 13839 (2017).
14. H. Das, V. Groh, C. Kuijl, M. Sugita, C. T. Morita, T. Spies, J. F. Bukowski, MICA engagement by human Vγ2Vδ2 T cells enhances their antigen-dependent effector function. *Immunity* **15**, 83–93 (2001).
15. J. Strid, O. Sobolev, B. Zafirova, B. Polic, A. Hayday, The intraepithelial T cell response to NKG2D-ligands links lymphoid stress surveillance to atopy. *Science* **334**, 1293–1297 (2011).
16. F. M. Wensveen, S. Valentic, M. Sestan, T. T. Wensveen, B. Polic, The "Big Bang" in obese fat: Events initiating obesity-induced adipose tissue inflammation. *Eur. J. Immunol.* **45**, 2446–2456 (2015).
17. Y. Chen, H. Wei, R. Sun, Z. Dong, J. Zhang, Z. Tian, Increased susceptibility to liver injury in hepatitis B virus transgenic mice involves NKG2D-ligand interaction and natural killer cells. *Hepatology* **46**, 706–715 (2007).
18. D. Sene, F. Levasseur, M. Abel, M. Lambert, X. Camous, C. Hernandez, V. Pene, A. R. Rosenberg, E. Jouvin-Marche, P. N. Marche, P. Cacoub, S. Caillat-Zucman, Hepatitis C virus (HCV) evades NKG2D-dependent NK cell responses through NS5A-mediated imbalance of inflammatory cytokines. *PLOS Pathog.* **6**, e1001184 (2010).
19. F. M. Wensveen, V. Jelencic, B. Polic, NKG2D: A master regulator of immune cell responsiveness. *Front. Immunol.* **9**, 441 (2018).
20. V. Jelencic, M. Sestan, I. Kavazovic, M. Lenartic, S. Marinovic, T. D. Holmes, M. Prchal-Murphy, B. Lisnic, V. Sexl, Y. T. Bryceson, F. M. Wensveen, B. Polic, NK cell receptor NKG2D sets activation threshold for the NCR1 receptor early in NK cell development. *Nat. Immunol.* **19**, 1083–1092 (2018).
21. S. Radaeva, R. Sun, B. Jaruga, V. T. Nguyen, Z. Tian, B. Gao, Natural killer cells ameliorate liver fibrosis by killing activated stellate cells in NKG2D-dependent and tumor necrosis factor-related apoptosis-inducing ligand-dependent manners. *Gastroenterology* **130**, 435–452 (2006).
22. D. E. Kleiner, E. M. Brunt, M. Van Natta, C. Behling, M. J. Contos, O. W. Cummings, L. D. Ferrell, Y.-C. Liu, M. S. Torbenson, A. Unalp-Arida, M. Yeh, A. J. McCullough, A. J. Sanyal; Nonalcoholic Steatohepatitis Clinical Research Network, Design and validation of a histological scoring system for nonalcoholic fatty liver disease. *Hepatology* **41**, 1313–1321 (2005).
23. N. Aizarani, A. Saviano, Sagar, L. Mailly, S. Durand, J. S. Herman, P. Pessaux, T. F. Baumert, D. Grün, A human liver cell atlas reveals heterogeneity and epithelial progenitors. *Nature* **572**, 199–204 (2019).
24. Q. M. Anstee, R. D. Goldin, Mouse models in non-alcoholic fatty liver disease and steatohepatitis research. *Int. J. Exp. Pathol.* **87**, 1–16 (2006).
25. J. R. Clapper, M. D. Hendricks, G. Gu, C. Wittmer, C. S. Dolman, J. Herich, J. Athanacio, C. Villescaz, S. S. Ghosh, J. S. Heilig, C. Lowe, J. D. Roth, Diet-induced mouse model of fatty liver disease and nonalcoholic steatohepatitis reflecting clinical disease progression and methods of assessment. *Am. J. Physiol. Gastrointest. Liver Physiol.* **305**, G483–G495 (2013).
26. M. Basaranoglu, B. A. Neuschwander-Tetri, Nonalcoholic fatty liver disease: Clinical features and pathogenesis. *Gastroenterol. Hepatol.* **2**, 282–291 (2006).
27. F. M. Wensveen, V. Jelencic, S. Valentic, M. Sestan, T. T. Wensveen, S. Theurich, A. Glasner, D. Mendrila, D. Stimac, F. T. Wunderlich, J. C. Bruning, O. Mandelboim, B. Polic, NK cells link obesity-induced adipose stress to inflammation and insulin resistance. *Nat. Immunol.* **16**, 376–385 (2015).
28. C. Savard, E. V. Tartaglione, R. Kuver, W. G. Haigh, G. C. Farrell, S. Subramanian, A. Chait, M. M. Yeh, L. S. Quinn, G. N. Ioannou, Synergistic interaction of dietary cholesterol and dietary fat in inducing experimental steatohepatitis. *Hepatology* **57**, 81–92 (2013).
29. B. Zafirova, S. Mandaric, R. Antulov, A. Krmpotic, H. Jonsson, W. M. Yokoyama, S. Jonjic, B. Polic, Altered NK cell development and enhanced NK cell-mediated resistance to mouse cytomegalovirus in NKG2D-deficient mice. *Immunity* **31**, 270–282 (2009).
30. S. Sheppard, J. Guedes, A. Mroz, A.-M. Zavitsanou, H. Kudo, S. M. Rothery, P. Angelopoulos, R. Goldin, N. Guerra, The immunoreceptor NKG2D promotes tumour growth in a model of hepatocellular carcinoma. *Nat. Commun.* **8**, 13930 (2017).
31. M. Lenartic, V. Jelencic, B. Zafirova, M. Ozanic, V. Marecic, S. Jurkovic, V. Sexl, M. Santic, F. M. Wensveen, B. Polic, NKG2D promotes B1a cell development and protection against bacterial infection. *J. Immunol.* **198**, 1531–1542 (2017).
32. Y. Cui, K. Franciszkiewicz, Y. K. Mburu, S. Mondot, L. Le Bourhis, V. Premel, E. Martin, A. Kachaner, L. Duban, M. A. Ingersoll, S. Rabot, J. Jaubert, J.-P. De Villartay, C. Soudais, O. Lantz, Mucosal-associated invariant T cell-rich congenic mouse strain allows functional evaluation. *J. Clin. Invest.* **125**, 4171–4185 (2015).
33. G. Eberl, R. Lees, S. T. Smiley, M. Taniguchi, M. J. Grusby, H. R. MacDonald, Tissue-specific segregation of CD1d-dependent and CD1d-independent NK T cells. *J. Immunol.* **162**, 6410–6419 (1999).
34. I. Sandrock, A. Reinhardt, S. Ravens, C. Binz, A. Wilharm, J. Martins, L. Oberdorfer, L. Tan, S. Lienenklaus, B. Zhang, R. Naumann, Y. Zhuang, A. Krueger, R. Forster, I. Prinz, Genetic models reveal origin, persistence and non-redundant functions of IL-17-producing γδ T cells. *J. Exp. Med.* **215**, 3006–3018 (2018).
35. I. Kavazovic, M. Lenartic, V. Jelencic, S. Jurkovic, N. A. W. Lemmermann, S. Jonjic, B. Polic, F. M. Wensveen, NKG2D stimulation of $CD8^+$ T cells during priming promotes their capacity to produce cytokines in response to viral infection in mice. *Eur. J. Immunol.* **47**, 1123–1135 (2017).
36. J. S. Lee, C. M. Tato, B. Joyce-Shaikh, M. F. Gulen, C. Cayatte, Y. Chen, W. M. Blumenschein, M. Judo, G. Ayanoglu, T. K. McClanahan, X. Li, D. J. Cua, Interleukin-23-independent IL-17 production regulates intestinal epithelial permeability. *Immunity* **43**, 727–738 (2015).
37. A. C. Kohlgruber, S. T. Gal-Oz, N. M. LaMarche, M. Shimazaki, D. Duquette, H.-F. Koay, H. N. Nguyen, A. I. Mina, T. Paras, A. Tavakkoli, U. von Andrian, A. P. Uldrich, D. I. Godfrey, A. S. Banks, T. Shay, M. B. Brenner, L. Lynch, γδ T cells producing interleukin-17A regulate adipose regulatory T cell homeostasis and thermogenesis. *Nat. Immunol.* **19**, 464–474 (2018).
38. L. Yang, Y. Jung, A. Omenetti, R. P. Witek, S. Choi, H. M. Vandongen, J. Huang, G. D. Alpini, A. M. Diehl, Fate-mapping evidence that hepatic stellate cells are epithelial progenitors in adult mouse livers. *Stem Cells* **26**, 2104–2113 (2008).
39. C. Khairallah, T. H. Chu, B. S. Sheridan, Tissue adaptations of memory and tissue-resident γδ T cells. *Front. Immunol.* **9**, 2636 (2018).
40. Y. Takahashi, Y. Soejima, T. Fukusato, Animal models of nonalcoholic fatty liver disease/nonalcoholic steatohepatitis. *World J. Gastroenterol.* **18**, 2300–2308 (2012).
41. N. Lopes, C. McIntyre, S. Martin, M. Raverdeau, N. Sumaria, A. C. Kohlgruber, G. J. Fiala, L. Z. Agudelo, L. Dyck, H. Kane, A. Douglas, S. Cunningham, H. Prendeville, R. Loftus, C. Carmody, P. Pierre, M. Kellis, M. Brenner, R. J. Arguello, B. Silva-Santos, D. J. Pennington, L. Lynch, Distinct metabolic programs established in the thymus control effector functions of γδ T cell subsets in tumor microenvironments. *Nat. Immunol.* **22**, 179–192 (2021).
42. M. J. McGeachy, D. J. Cua, S. L. Gaffen, The IL-17 family of cytokines in health and disease. *Immunity* **50**, 892–906 (2019).
43. A. Wieckowska, B. G. Papouchado, Z. Li, R. Lopez, N. N. Zein, A. E. Feldstein, Increased hepatic and circulating interleukin-6 levels in human nonalcoholic steatohepatitis. *Am. J. Gastroenterol.* **103**, 1372–1379 (2008).
44. I. Mikolasevic, V. Domislovic, T. Turk Wensveen, B. Delija, M. Klapan, T. Juric, A. Lukic, A. Mijic, N. Skenderevic, P. Puz, A. Ostojic, Z. Krznaric, D. Radic-Kristo, T. Filipec Kanizaj, D. Stimac, Screening for nonalcoholic fatty liver disease in patients with type 2 diabetes mellitus using transient elastography–A prospective, cross sectional study. *Eur. J. Intern. Med.* **82**, 68–75 (2020).
45. T. D. Huang, J. Behary, A. Zekry, Non-alcoholic fatty liver disease: A review of epidemiology, risk factors, diagnosis and management. *Intern. Med. J.* **50**, 1038–1047 (2020).
46. M. T. Bilotta, M. P. Abruzzese, R. Molfetta, G. Scarno, C. Fionda, A. Zingoni, A. Soriani, T. Garofalo, M. T. Petrucci, M. R. Ricciardi, R. Paolini, A. Santoni, M. Cippitelli, Activation of liver X receptor up-regulates the expression of the NKG2D ligands MICA and MICB in multiple myeloma through different molecular mechanisms. *FASEB J.* **33**, 9489–9504 (2019).
47. A. Katz, C. Udata, E. Ott, L. Hickey, M. E. Burczynski, P. Burghart, O. Vesterqvist, X. Meng, Safety, pharmacokinetics, and pharmacodynamics of single doses of LXR-623, a novel liver X-receptor agonist, in healthy participants. *J. Clin. Pharmacol.* **49**, 643–649 (2009).
48. T. G. Kirchgessner, P. Sleph, J. Ostrowski, J. Lupisella, C. S. Ryan, X. Liu, G. Fernando, D. Grimm, P. Shipkova, R. Zhang, R. Garcia, J. Zhu, A. He, H. Malone, R. Martin, K. Behnia, Z. Wang, Y. C. Barrett, R. J. Garmise, L. Yuan, J. Zhang, M. D. Gandhi, P. Wastall, T. Li, S. Du, L. Salvador, R. Mohan, G. H. Cantor, E. Kick, J. Lee, R. J. A. Frost, Beneficial and adverse effects of an LXR agonist on human lipid and lipoprotein metabolism and circulating neutrophils. *Cell Metab.* **24**, 223–233 (2016).

49. D. A. Giles, M. E. Moreno-Fernandez, S. Divanovic, IL-17 axis driven inflammation in non-alcoholic fatty liver disease progression. *Curr. Drug Targets* **16**, 1315–1323 (2015).
50. I. T. W. Harley, T. E. Stankiewicz, D. A. Giles, S. Softic, L. M. Flick, M. Cappelletti, R. Sheridan, S. A. Xanthakos, K. A. Steinbrecher, R. B. Sartor, R. Kohli, C. L. Karp, S. Divanovic, IL-17 signaling accelerates the progression of nonalcoholic fatty liver disease in mice. *Hepatology* **59**, 1830–1839 (2014).
51. A. L. Gomes, A. Teijeiro, S. Buren, K. S. Tummala, M. Yilmaz, A. Waisman, J. P. Theurillat, C. Perna, N. Djouder, Metabolic inflammation-associated IL-17A causes non-alcoholic steatohepatitis and hepatocellular carcinoma. *Cancer Cell* **30**, 161–175 (2016).
52. A. M. McGinley, C. E. Sutton, S. C. Edwards, C. M. Leane, J. DeCourcey, A. Teijeiro, J. A. Hamilton, L. Boon, N. Djouder, K. H. G. Mills, Interleukin-17A serves a priming role in autoimmunity by recruiting IL-1β-producing myeloid cells that promote pathogenic T cells. *Immunity* **52**, 342–356.e6 (2020).
53. M. Babic, C. Dimitropoulos, Q. Hammer, C. Stehle, F. Heinrich, A. Sarsenbayeva, A. Eisele, P. Durek, M. F. Mashreghi, B. Lisnic, J. Van Snick, M. Lohning, S. Fillatreau, D. R. Withers, N. Gagliani, S. Huber, R. A. Flavell, B. Polic, C. Romagnani, NK cell receptor NKG2D enforces proinflammatory features and pathogenicity of Th1 and Th17 cells. *J. Exp. Med.* **217**, e20190133 (2020).
54. M. E. Moreno-Fernandez, D. A. Giles, J. R. Oates, C. C. Chan, M. Damen, J. R. Doll, T. E. Stankiewicz, X. Chen, K. Chetal, R. Karns, M. T. Weirauch, L. Romick-Rosendale, S. A. Xanthakos, R. Sheridan, S. Szabo, A. S. Shah, M. A. Helmrath, T. H. Inge, H. Deshmukh, N. Salomonis, S. Divanovic, PKM2-dependent metabolic skewing of hepatic Th17 cells regulates pathogenesis of non-alcoholic fatty liver disease. *Cell Metab.* **33**, 1187–1204.e9 (2021).
55. X. Li, R. Bechara, J. Zhao, M. J. McGeachy, S. L. Gaffen, IL-17 receptor-based signaling and implications for disease. *Nat. Immunol.* **20**, 1594–1602 (2019).
56. J. R. Lukens, M. J. Barr, D. D. Chaplin, H. Chi, T. D. Kanneganti, Inflammasome-derived IL-1β regulates the production of GM-CSF by $CD4^+$ T cells and γδ T cells. *J. Immunol.* **188**, 3107–3115 (2012).
57. R. M. Onishi, S. L. Gaffen, Interleukin-17 and its target genes: Mechanisms of interleukin-17 function in disease. *Immunology* **129**, 311–321 (2010).
58. A. D. Kim, S. E. Kim, A. Leszczynska, B. Kaufmann, A. Reca, D. J. Kim, A. E. Feldstein, Dual role of neutrophils in modulating liver injury and fibrosis during development and resolution of diet-induced murine steatohepatitis. *Sci. Rep.* **11**, 24194 (2021).
59. S. Hwang, H. Yun, S. Moon, Y. E. Cho, B. Gao, Role of neutrophils in the pathogenesis of nonalcoholic steatohepatitis. *Front. Endocrinol.* **12**, 751802 (2021).
60. M. A. Freitas-Lopes, K. Mafra, B. A. David, R. Carvalho-Gontijo, G. B. Menezes, Differential location and distribution of hepatic immune cells. *Cells* **6**, 48 (2017).
61. M. Sasso, M. Beaugrand, V. De Ledinghen, C. Douvin, P. Marcellin, R. Poupon, L. Sandrin, V. Miette, *Ultrasound Med. Biol.* 362010), 1825–1835.
62. V. W. Wong, J. Vergniol, G. L. Wong, J. Foucher, A. W. Chan, F. Chermak, P. C. Choi, W. Merrouche, S. H. Chu, S. Pesque, Liver stiffness measurement using XL probe in patients with nonalcoholic fatty liver disease. *Am. J. Gastroenterol.* **107**, 1862–1871 (2012).
63. V. W. Wong, J. Vergniol, G. L. Wong, J. Foucher, H. L. Chan, B. Le Bail, P. C. Choi, M. Kowo, A. W. Chan, W. Merrouche, Diagnosis of fibrosis and cirrhosis using liver stiffness measurement in nonalcoholic fatty liver disease. *Hepatology* **51**, 454–462 (2010).
64. M. Charni-Natan, I. Goldstein, Protocol for primary mouse hepatocyte isolation. *STAR Protocols* **1**, 100086 (2020).
65. J. M. Pappachan, S. Babu, B. Krishnan, N. C. Ravindran, Non-alcoholic fatty liver disease: A clinical update. *J. Clin. Transl. Hepatol.* **5**, 384–393 (2017).

Acknowledgments: We thank S. Slavić Stupac, M. Samsa, A. Miše, and V. Jeleňić for technical support and handling of mice. We thank S. Jonjić for providing us with essential research reagent. We thank O. Lantz, V. Sexl, D. Liottman, and M. Colonna for providing the mouse lines. We thank the NIH Tetramer core facility for providing the reagents. We acknowledge the support of the EMBL Metabolomics Core Facility (MCF) in the acquisition and analysis of LC-MS data. **Funding:** This work was supported by grants of the University of Rijeka (18-152-1301 to F.M.W., 18-89-1224 to B.P., and 18-117-1256 to T.T.W.), a grant of the Faculty of Fedicine Rijeka to M.L. (100.21.0006) and Croatian Science Foundation (IP-2016-06-9306 and IPCH-2020-10-8440 to B.P., IP-2016-06-8027 and IP-CORONA-2020-04-2045 to F.M.W., and IP-2020-02-7928 to T.T.W.), the European Regional Development Fund (KK.01.1.1.01.0006) to B.P., and the Deutsche Forschungsgemeinshaft (318346496-SFB1292/2 and 490846870-TRR355/1) to A.W. **Author contributions:** S.M., M.L., and K.M. designed and performed experiments and cowrote the article. M.Š., I.K., A.B., M.C.B., M.K., L.R, C.S., and G.L. performed experiments; T.T.W. and I.M. collected patient material; D.F.Č. and L.B.-Z. analyzed patient material; A.S., A.W., S.T., B.B., and A.H. provided reagents and helped with the design of the study; and B.P. and F.M.W. supervised the project, designed experiments, and wrote the paper. **Competing interests:** A.H. is an equity holder in and consultant to GammaDelta Therapeutics, Adaptate Biotherapeutics, and ImmunoQure AG. All other authors declare that they have no competing interests. **Data and materials availability:** All unique materials and reagents will be made available by the corresponding author upon reasonable request. RNA-sequencing datasets generated in this paper are available under accession code GSE200482.

Submitted 24 May 2022
Resubmitted 28 April 2023
Accepted 23 August 2023
Published 29 September 2023
10.1126/sciimmunol.add1599

Science Immunology

NKG2D-mediated detection of metabolically stressed hepatocytes by innate-like T cells is essential for initiation of NASH and fibrosis

Sonja Marinovi#, Maja Lenarti#, Karlo Mladeni#, Marko Šestan, Inga Kavazovi#, Ante Beni#, Mia Krapi#, Lukas Rindlisbacher, Maja Cokari# Brdov#ak, Colin Sparano, Gioana Litscher, Tamara Turk Wensveen, Ivana Mikolaševi#, Dora F#kar #upi#, Lidija Bili#-Zulle, Aleksander Steinle, Ari Waisman, Adrian Hayday, Sonia Tugues, Burkhard Becher, Bojan Poli#, and Felix M. Wensveen

Sci. Immunol. **8** (87), eadd1599. DOI: 10.1126/sciimmunol.add1599

Science Immunology (ISSN 2470-9468) is published by the American Association for the Advancement of Science. 1200 New York Avenue NW, Washington, DC 20005. The title *Science Immunology* is a registered trademark of AAAS.